sustainability

MDPI

Review

Recent Advances in Capacitive Deionization: Research Progress and Application Prospects

Meijun Liu [1], Mengyao He [1], Jinglong Han [2], Yueyang Sun [1], Hong Jiang [3], Zheng Li [1], Yuna Li [1] and Haifeng Zhang [1,*]

[1] School of Chemical Engineering, Northeast Electric Power University, Jilin 132012, China
[2] School of Civil & Environmental Engineering, Harbin Institute of Technology, Shenzhen 518055, China
[3] Northeast Electric Power Design Institute Co., Ltd. of China Power Engineering Consulting Group, Changchun 130000, China
* Correspondence: zhfeepu@163.com; Tel.: +86-0432-64806371

Abstract: With the increasing global water shortage issue, the development of water desalination and wastewater recycling technology is particularly urgent. Capacitive deionization (CDI), as an emerging approach for water desalination and ion separation, has received extensive attention due to its high ion selectivity, high water recovery, and low energy consumption. To promote the further application of CDI technology, it is necessary to understand the latest research progress and application prospects. Here, considering electric double layers (EDLs) and two typical models, we conduct an in-depth discussion on the ion adsorption mechanism of CDI technology. Furthermore, we provide a comprehensive overview of recent advances in CDI technology optimization research, including optimization of cell architecture, electrode material design, and operating mode exploration. In addition, we summarize the development of CDI in past decades in novel application fields other than seawater desalination, mainly including ionic pollutant removal, recovery of resource-based substances such as lithium and nutrients, and development of coupling systems between CDI and other technologies. We then highlight the most serious challenges faced in the process of large-scale application of CDI. In the conclusion and outlook section, we focus on summarizing the overall development prospects of CDI technology, and we discuss the points that require special attention in future development.

Keywords: capacitive deionization (CDI); desalination; electrosorption; system architectures; electrode materials; energy efficiency

check for updates

Citation: Liu, M.; He, M.; Han, J.; Sun, Y.; Jiang, H.; Li, Z.; Li, Y.; Zhang, H. Recent Advances in Capacitive Deionization: Research Progress and Application Prospects. *Sustainability* **2022**, *14*, 14429. https://doi.org/10.3390/su142114429

Academic Editors: Deepak Pant and Giovanni De Feo

Received: 20 August 2022
Accepted: 1 November 2022
Published: 3 November 2022

Publisher's Note: MDPI stays neutral with regard to jurisdictional claims in published maps and institutional affiliations.

Copyright: © 2022 by the authors. Licensee MDPI, Basel, Switzerland. This article is an open access article distributed under the terms and conditions of the Creative Commons Attribution (CC BY) license (https://creativecommons.org/licenses/by/4.0/).

1. Introduction

Due to rapid industrialization, climate change, population explosion and the spread of water pollution, natural freshwater resources can no longer meet the growing global demand for clean water [1]. However, freshwater accounts for only 2.5% of total global water resources, and they are mostly stored in the form of glacial water or deep groundwater [2]. Seawater and brackish water with abundant reserves cannot be directly used as domestic water. Therefore, desalination technology is considered to be one of the most effective solutions to alleviate the water shortage issue [3]. Currently, desalination technologies can be broadly classified into three categories according to the driving force to separate ions from water. The first category is the conventional thermally driven desalination technology, which involves evaporating the feedwater and the subsequent condensation of the vapor to obtain distilled water (Figure 1a) [4]. The widely used thermal desalination techniques including multistage flash (MSF), multiple-effect distillation (MED), and mechanical vapor compression (MVC). [5]. In addition, membrane distillation is based on the fractional pressure-driven vapor transport of hydrophobic membranes [6], and it represents an emerging thermally driven desalination technology. Due to the inherent limitations of energy

efficiency, the application of thermally driven desalination technologies in the market has been decreasing over the past few decades [7]. The second category is pressure-driven desalination technology represented by reverse osmosis (RO). When the pressure is greater than the osmotic pressure of the aqueous solution, the water in the solution is pushed across the semipermeable membrane, while the solute is expelled to the other side of the semipermeable membrane (Figure 1b) [8]. RO has near-perfect repulsion to charged ions and has been widely used in seawater and brackish water desalination. The third category is electro-desalination technology, which is driven by an external electric field. The most typical electrolytic desalination technology is electrodialysis (ED) (Figure 1c), in which ions are selectively passed through ion-exchange membranes (IEMs) under an applied electric field and delivered to a concentrated stream, thus effectively removing the ions of the feedwater [9]. Since the cost of IEMs is much higher than that of RO membranes, and the high-voltage operation mode leads to the consumption of electricity via Faradaic reactions, ED technology suffers from inherently low energy efficiency, which makes it not as widely used in desalination as RO. Although the existing technologies play a pivotal part in the development of the desalination field, the defects are also relatively obvious. In addition, traditional technologies usually do not have the ability to selectively remove ionic substances in water, which limits their application in specific pollutant (heavy metals, etc.) removal or resource (lithium, nutrients, etc.) recovery. With the increasing demand for fresh water, it is urgent to develop a desalination technology with a better desalination effect, higher energy efficiency, and long-term stable operation.

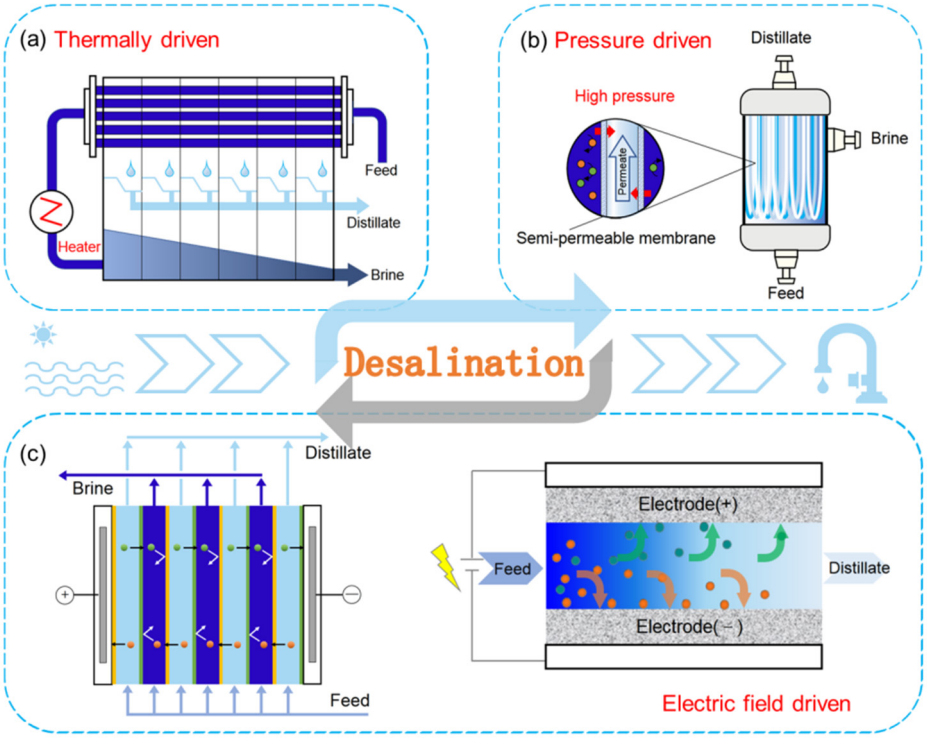


Figure 1. Schematic representation of three main types of desalination processes: (**a**) thermally driven desalination, such as MED, MSF, MVC, or membrane distillation (not shown here); (**b**) pressure-driven desalination, such as RO or NF; (**c**) electric field-driven desalination (or electrochemical desalination), such as CDI or ED.

In 1967, Murphy and Caudle created the first CDI cell with porous carbon material as electrodes [10], which would produce a positive and negative charge, respectively, under an applied potential (Figure 2a). Compared with RO, CDI usually does not require membrane modules, and the limitations for influent quality are much less than those of RO. It not only simplifies the complex pretreatment process, but also reduces the risk of degradation of desalination efficiency caused by membrane fouling. The ion removal

mechanism of traditional CDI is to form electric double layers (EDLs) on the surface of carbon electrodes with large specific surface area [11]. Two models are mainly used in the current study. Among them, the Gouy–Chapman–Stern (GCS) model is suitable for carbon electrode materials with a large pore and suitable for quantifying the effects of pore size, carbon-specific surface area, and the feed concentration on the desalination performance [12–14]. However, the EDLs would overlap inside the microporous carbon electrode (pore size < 1 nm) according to the GCS model. Alternatively, the modified Donnan model [15] can be used to describe the electric double-layer structure in the micropore and serve as the modeling basis for the CDI desalination system [16–18]. The optimized model construction lays a certain theoretical basis for the research of CDI systems in the application of desalination.

In order to further optimize the ion removal performance of the CDI system, researchers have carried out comprehensive research on the aspects of cell configuration, electrode material design, and operation mode optimization. Due to the energy efficiency of the system being affected by the co-ion expulsion of classic CDI, Lee et al. introduced IEMs alongside electrodes and proposed the concept of membrane capacitive deionization (MCDI) [19]. Under the selective permeation of ions by IEMs, the charge on the electrode surface can be used for the attraction of counter ions without spending on the repulsion of co-ions, which effectively improves the salt removal ability and the energy efficiency of the system. In addition, the electrode adsorption and desorption processes of traditional CDI and MCDI are separated, and the intermittent electrode regeneration process makes the control process more complicated. Jeon et al. introduced the activated carbon slurry electrode into the CDI system and proposed the concept of flow electrode capacitance deionization (FCDI), which enables achieving continuous desalination operation [20]. The development of early CDI and its derivative systems was mainly based on carbon materials, which are the most mature CDI electrode materials due to their cheap and easy availability, good electrical conductivity, abundant porous structure, and high specific surface area. Carbon material electrodes that have been reported for use in CDI systems including carbon nanotubes [21], graphene [22], mesoporous carbon [23], and carbon aerogels [24]. However, carbon materials have limited charge storage capacity (100–200 $F \cdot g^{-1}$) [25] and cannot achieve selective removal of ions. Although the adverse effect of co-ion repulsion can be mitigated by the introduction of IEMs, there is a contact resistance between the IEMs and the electrode, which may also bring membrane fouling to the CDI cell. In order to further improve the deionization performance of the CDI system, the researchers introduced Faraday electrodes, which constituted a hybrid capacitive demineralization (HCDI) [26] with superior ion removal performance. Unlike traditional CDI, the Faraday electrode achieves ion capture by intercalating ions between electrode material layers, inside the lattice, or through redox reactions with ions, which effectively reduces ion migration resistance, so as to improve energy efficiency. In recent decades, intercalated electrode materials (including two-dimensional MXenes and three-dimensional PBAs) [27,28], polymer electrode materials (polyaniline (PANI) and polypyrrole (PPy)), etc. have been used as Faraday electrodes. Materials have been used in the field of CDI and have made significant progress. However, the selective adsorption performance of existing electrode materials for target ions needs to be further improved, and the interaction mechanism between the electrode interface structure and specific ions needs to be further studied.

Recently, CDI has gradually expanded broader application fields from the initial application of seawater and brackish water desalination, especially for the selective removal of ionic pollutants in the water environment, including water softening [29] and removal of toxic heavy metals [30], as well as the selective recovery of resource-based ions, including the recycling of high-valent elements lithium [31–37] and nutrient ions [38,39]. In addition to ionic species, CDI systems have been applied for the capture of CO_2 through the conversion of dissolution equilibrium and adsorption equilibrium, and this progress provides a new idea for the capture of soluble gas molecules [40,41]. Since CDI technology is only suitable for the removal of ionic substances, the ability to remove neutral organic substances

is limited. To further explore wider applications, researchers coupled CDI technology with other techniques, which effectively compensated for the limitations of the two techniques and resulted in better performance than the single technique [42]. Although the existing application research has achieved remarkable results, most examples are limited to the laboratory scale. Due to the fact that the feed stream in practical applications is usually composed of complex components and the water quality fluctuates greatly, further in-depth research is still required before CDI technology is promoted for application.

In this review, we first outline the mechanism of ion removal during CDI desalination and focus on two adsorption models. Then, the current research progress of CDI technology optimization is reviewed, and strategies for optimizing CDI systems from the perspectives of cell configuration, electrode material design, and operation mode are summarized. Lastly, some emerging fields in which CDI technology is currently applied are summarized, and some guiding opinions for future development are put forward.

2. Reaction Mechanism of CDI

The reaction mechanism of CDI for desalination is an "electrosorption" process, in which the counter ions are fixed to the EDL under an electric field, while the co-ions are repelled and moved away from the surface of the electrode (Figure 2b) [43,44]. Among them, some of the counter ions are not concentrated on the electrode surface, but diffuse on the layer close to the electrode. The formed region is called the Gouy–Chapman (GC) layer, and its ion concentration decreases gradually with increasing distance from the electrode surface. The inner layer that exists between the diffusion layer and the electrode is called the Stern layer, which is electrically neutral [17].

When the pore size of the porous electrode material is much larger than the Debye length, it can be assumed that the EDLs do not overlap. In this case, the classical GCS model is usually used to study the ion distribution at the plane or electrode interface. At present, most of the research on EDL focuses on the amount of charge stored in the EDL. However, the CDI system focuses on the number of ions stored in the EDL, where the related research is scarce. The EDL model of charge storage and ion storage is the same. At low voltage, the capacitance for charge storage is not zero, while the capacitance for ion storage is zero, resulting in a system with a current efficiency close to zero. Therefore, how to effectively improve the current efficiency of the CDI system under low-voltage conditions and achieve low energy consumption for desalination is the key issue in this field. During the charging process, ions are separated from the electrolyte and stored in EDLs on the electrode surface; subsequently, during the discharging process, the ion concentration of the solution increases with the release of the stored ions into the electrolyte. The concentration difference generated in the discharge process is accompanied by the release of energy, which can be transferred to an adjacent cell or individual supercapacitor and recovered by the converter [45,46].

When the GCS model was applied to CDI experiments with porous carbon electrodes, the theoretical amount of co-ion expelled from the EDLs exceeded the amount of co-ion originally present in the electrode under high-voltage conditions [13]. This is caused by the pore size of the electrode micropores being smaller than the Debye length and resulting in the overlap of EDLs. Applying the modified Donnan model (Figure 2c) to the CDI system can effectively avoid the limitation and accurately describe important theoretical data such as salt adsorption and charge storage balance in CDI [47–51]. When the Debye length is much larger than the electrode micropores size (about 1–2 nm), the EDLs inside the carbon electrode particles are highly overlapped, and it can be considered that the potentials at different positions in the micropores are consistent. Donnan theory assumes that the properties of the diffusion layer are independent of its distance from the Stern plane, but the rest of the Donnan model is similar to that of the GCS model.

Although the Donnan model is mathematically simpler, it cannot clearly describe the detailed data of salt adsorption and charge distribution in microporous carbon; thus, the Donnan model usually needs to be modified in two ways [52]. The first modification

method is to introduce a Stern layer between the charges in the carbon matrix and the electrolyte ions in the electrode micropores. Since ions have different radii under hydration/dehydration conditions, the electronic charges are not completely located at the edge of the carbon material, and there is a certain "roughness" at the interface between the carbon electrode and the electrolyte, the ionic charges in the Stern layer cannot be infinitely close to the electronic charges. The second correction method is to introduce chemical gravitational energy during the transfer of ions from the outside to the inside of the carbon electrode particles. This approach takes into account that, in the absence of electric charges, ions enter the inside of the electrode pores under the action of non-electrostatic attraction [53]. When the electrode has macropores and micropores, both of which are filled with electrolytes, the ion concentration in the micropores is assumed to be equal to the local average by the Donnan model, while the macropores present electrically neutral. When the salt ion concentration reaches a certain value, the excess ionic charge in the micropores is compensated for by the charge in the carbon matrix. In general, the GCS model and the modified Donnan model are effective tools to study CDI systems, which can provide a clearer understanding of the equilibrium and ion transport characteristics in the reaction system. They provide a general concept and theoretical basis for studying the CDI reaction mechanism.

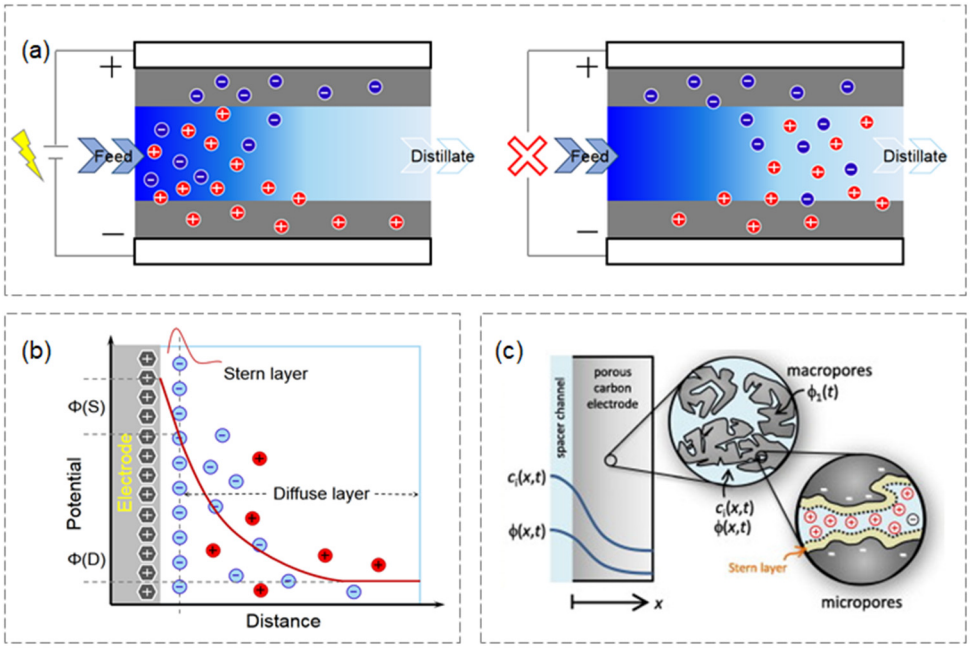


Figure 2. (**a**) Schematic diagram of the desalination mechanism of the CDI process; (**b**) schematic diagram of the EDLs of single-plane based on GCS theory. Adapted with permission from Ref. [54]. 2020, Liu X and from Ref. [55]. 2017, Xu X; (**c**) Donnan model (electrode two-hole model) Adapted with permission from Ref. [17]. 2013, Porada S.

3. Optimization Strategies of CDI

3.1. Cell Architecture

Although CDI has significant advantages among desalination technologies, there is a tradeoff between ion removal rate and energy efficiency. In order to further promote the application of CDI, researchers have made various attempts in cell architecture. At present, cell architectures that have attracted the most attention include classic CDI, membrane CDI (MCDI), flow-electrode CDI (FCDI), and hybrid CDI (HCDI). Figure 3 is a schematic diagram of these cell architectures.

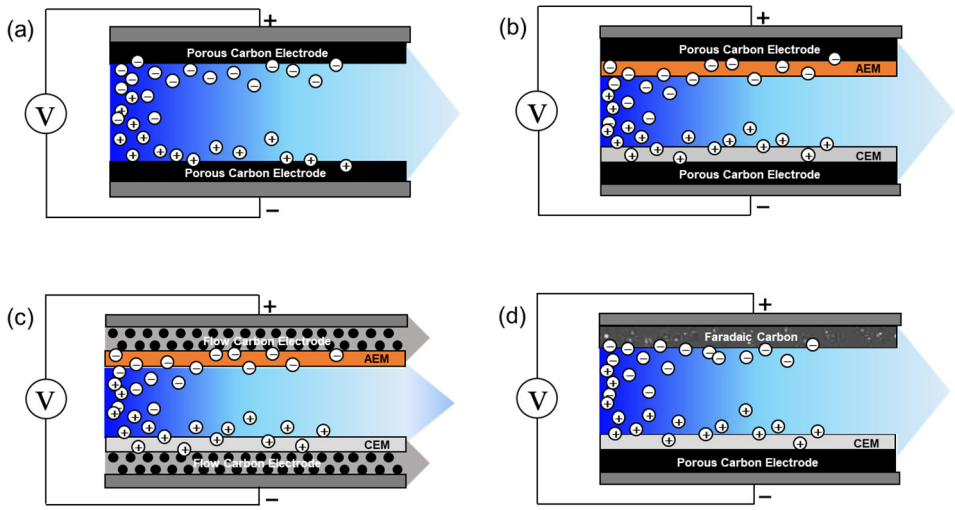


Figure 3. (**a**) Classic capacitive deionization (CDI); (**b**) membrane capacitive deionization (MCDI). (**c**) flow electrode capacitive deionization (FCDI); (**d**) hybrid Capacitive deionization (HCDI).

3.1.1. Classic CDI

Founded on the principle of ion electrosorption, classic CDI (Figure 3a), which originated in the 1960s [10], consists of a pair of carbon electrodes with porous structure separated by a nonconductive spacer. Due to its simple structure and ease of establishment, the classic CDI has been widely used in industry [56,57]. At present, the research of classic CDI systems is mainly focused on theoretical modeling [13,16,17], construction of novel cell architectures [17,26,55], electrode material design [23,58,59], and energy recovery [60,61].

The theoretical potential difference for electrochemical water splitting is 1.23 V. In order to avoid charge depletion by parasitic water splitting (hydrogen and oxygen evolution reactions) and other side reactions from consuming electric charge [62], the operating voltage of classic CDI is usually $\leq$1.2 V [63]. Compared with electrodialysis desalination technology, the low-voltage operation mode effectively improves energy efficiency, making CDI the most promising electrically driven desalination technology. In addition to the adsorption of counter ions, the electrode of classic CDI will repel co-ions back to the reaction channel, thus reducing the desalination efficiency of the CDI system. Especially in high-concentration brine, the energy consumption of the co-ion exclusion process in the adsorption stage is higher, resulting in lower current efficiency. Therefore, classic CDI is only suitable for the treatment of low-concentration brine [64].

Carbon materials used in classic CDI have porous structures, various surface functional groups, and limited active sites, making them ideal organic adsorbents [65]. The effective adsorption characteristic also makes the porous carbon electrodes sensitive to organics in the feed stream [66], which might lead to a significant reduction in the removal rates under long-term operating conditions [67]. In addition, the porous carbon materials used in classic CDI have a fixed adsorption active area, which limits the total adsorption capacity of electrodes [17,68]. Therefore, how to improve the salt adsorption capacities (SACs) of the CDI system has become the key issue of the related research.

3.1.2. Membrane Capacitive Deionization (MCDI)

By introducing IEMs on the surface of CDI electrodes, the constructed cell architecture is called MCDI (Figure 3b). Since IEMs are semipermeable to charged ions, an AEM allows only anions to pass through, while a CEM allows only cations to pass through. Placing AEM in front of the anode and CEM in front of the cathode can weaken the co-ion repulsion effect on the surface of the electrode. In MCDI, the co-ion expelled during the adsorption process is not trapped in the water channel by the IEMs. Moreover, to achieve charge balance, the trapped co-ion within the electrode can go a step further by attracting more

and more counter ions into the electrode; thus, MCDI can achieve higher total salt removal than classic CDI.

Compared with the classic CDI, MCDI has a larger ion adsorption capacity, higher charge efficiency [17,18], more diverse operation conditions, and better anti-fouling performance, which is due to the ion-selective migration in MCDI with the IEMs [17,19,47,69,70]. Biesheuvel et al. approved through a laboratory-scale study that MCDI increased the salt removal rate by 20% compared with classic CDI when treating a 1200 ppm NaCl solution [69]. Another lab-scale study showed that MCDI performed nearly 30% better salt removal rate than classic CDI when treated with 400 ppm NaCl [71]. Furthermore, compared with classic CDI, MCDI cells have more diverse operation modes. In addition to the constant-voltage (CV) mode, MCDI can use the constant-current (CC) mode for desalination operation. When the adsorbed ions on the fixed electrode are saturated, the reverse voltage desorption (RVD) mode can be used to accelerate the desorption of ions inside the electrode (see Section 3.3 for the optimization of the operation mode). Moreover, IEMs have been shown to be effective in extending electrode lifetime by reducing the oxidation of anodic carbon electrodes [72,73].

Although the introduction of IEMs significantly improved the desalination performance, MCDI still uses static electrodes. The pore structure on the fixed electrode for storing ions is limited, and the saturated electrode limits its total SACs in the adsorption stage [17,74]. Therefore, MCDI is only suitable for treating low and medium concentrations (about 3000–4000 $mg \cdot L^{-1}$) of ions and is not suitable for treating industrial brine with high ion concentration (>10,000 ppm). In addition, since the saturated electrode needs to be regenerated, the adsorption and desorption stages are separated, resulting in the discontinuous operation of both classic CDI and MCDI systems [55,75]. Although MCDI currently has an industrial scale, its stability under long-term application still needs to be verified [76,77]. In addition, the fouling mechanism of IEMs under long-term operating conditions still needs further research.

3.1.3. Flow Electrode Capacitive Deionization (FCDI)

During the operation of classic CDI and MCDI, the ion adsorption and electrode regeneration processes need to be alternated. This noncontinuous operation mode requires the design of a complex control mode. During the switching of the potential direction, a part of the diluted water will be lost, which will affect the water recovery rate. In order to solve the limitations caused by the fixed electrodes, Jeon et al. first proposed the concept of FCDI in 2013 (Figure 3c) [20]. The slurry electrode used in FCDI consists of activated carbon particles with a specific surface area of about 3200 m^2/g, and it has a higher electrosorption capacity (>20 $mg \cdot g^{-1}$) than MCDI (average 1–11 $mg \cdot g^{-1}$). The conductive slurry is continuously pumped into the electrode chamber of the FCDI cell, and the regeneration of the electrode is carried out in a separate system outside the FCDI cell.

The flow electrode in FCDI has a higher specific surface area than the fixed electrode, which leads to better desalination performance of FCDI for high-concentration brine. Studies have proven that FCDI has a high desalination performance for brines with a high total dissolved solid concentration (TDS) of seawater (about 35,000 $mg \cdot L^{-1}$) [78]. Unlike classic CDI and MCDI, the flow electrode can be recycled outside FCDI batteries, and the desorption and adsorption processes in the system can be performed separately. It enables continuous desalination operation of the FCDI system and effectively improves the water recovery rate. When a voltage is applied, the charged ions tolerate the IEMs and are fixed to the surface of the suspended carbon particles within the flow electrode. The effused flow electrodes from the anode and cathode chambers of the FCDI cell are mixed and regenerated in an external system. Furthermore, the desalination capacity of the FCDI system can be extended by increasing the number of flow electrodes [20]. The significant advantages of the FCDI system make it a great potential for industrial-scale desalination applications [20,79].

Early research about FCDI mainly focused on increasing the ion loading of carbon electrode materials in FCDI, thereby improving the desalination efficiency of the system. Since 2016, some of the research has turned to cell architecture design and operation mode research. The FCDI cell architectures that have been developed so far include single-module FCDI batteries [80], dual-module FCDI batteries [81], and two-step regenerative FCDI batteries with energy recovery [82]. In addition to basic and lab-scale studies, it is particularly important to evaluate the feasibility of FCDI systems in various industrial applications. In general, FCDI research is still at its lab scale, and energy consumption optimization is required in the case of high-concentration TDS feed (>2000 ppm) [83–85]. Further research on the long-term operational stability of the system should also be carried out [84,86], and its feasibility in large-scale desalination (>125 $mL \cdot min^{-1}$) needs to be evaluated [87–89]. The mechanism of electrode or IEM scaling in FCDI systems has not been extensively studied; thus, any analysis and development are still needed before FCDI technology can be widely used.

3.1.4. Hybrid Capacitive Deionization (HCDI)

In addition to flow electrodes, the introduction of Faraday electrodes is one of the important ways to improve the ion adsorption capacity of CDI electrodes. Since the target ions of the two electrodes in the CDI system are different, various Faraday electrodes are used to selectively adsorb cations or anions, respectively. Na^+ intercalation materials can be used as CDI cathodes, such as sodium transition metal oxides, polyanionic compounds, or metal hexacyanometalates, to adsorb/desorb Na^+ through intercalation/release. In contrast, CDI anodes usually use conversion materials (such as Ag/AgCl or Bi/BiOCl) to capture Cl^- [90,91]. In 2012, Pasta et al. first carried out the research on the CDI system with double Faraday electrodes ($Na_2Mn_5O_{10}$//AgCl) [90]. The introduction of the Faraday electrodes can effectively reduce the co-ion repulsion effect and has shown the capacity for desalination of low-concentration and high-concentration brines (such as brackish water or even seawater) [92]. The concept of HCDI was first proposed in 2014 by Yoon et al., which refers to a CDI system consisting of two different Faraday electrodes, or a Faraday electrode and a capacitive carbon electrode (Figure 3d) [26]. A Faraday electrode with high Na^+ storage capacity was selected as the cathode, and a porous carbon electrode coupled with AEM was used as the anode for selectively adsorb Cl^-. The constructed HCDI ($Na_4Mn_9O_{18}$//AC-AEM) performs a high desalination capacity of 31.2 $mg \cdot g^{-1}$, which is more than twice that of the classic CDI (13.5 $mg \cdot g^{-1}$).

Due to high energy density, high conductivity, high Faraday reaction, and low cost, transition metal oxides (TMOs) are ideal HCDI cathode materials and have been used as electrode materials for energy storage devices such as secondary batteries and supercapacitors. Among them, MnO_2, as a typical TMO, has a high theoretical capacitance (specific capacitance is greater than 1300 $F \cdot g^{-1}$, and volume specific capacitance is approximately 290 $F \cdot g^{-1}$), and its application in HCDI systems has received further attention from researchers. Hand et al. synthesized a MnO_2 electrode using the electrodeposition technique, and the assembled HCDI system exhibited good desalination performance (2.29 mmol $Na^+ \cdot g^{-1}$, charging efficiency of 0.95) [93]. Due to the asymmetric architecture of HCDI, the desalination capability and stability of the system composed of MnO_2//C electrodes are restricted by the less reactive carbon anode. To handle this drawback, Qiu et al. developed an inverted HCDI system [94]. By combining a MnO_2 anode with a positively charged anion-selective activated carbon (AC) material, the created HCDI cell also possesses the advantages of a selective carbon anode (reducing the negative effects of co-ion rejection) and the advantages of Faraday anodes (wide operational voltage and no anode corrosion). The salt ion adsorption capacity is 14.9 $mg \cdot g^{-1}$, and the desalination capacity of 95.4% is maintained after 350 adsorption/desorption cycles. Additionally, several different TMOs, such as Co_3O_4, ZrO_2 [95], Fe_3O_4 [96], and RuO_2 [97], have been widely explored as HCDI electrodes in recent years. However, the electrical conductivity of TMOs is typically poor, and carbon materials are usually used as composite additives. In addition, the structural

stability of some TMO electrodes is poor, and it may dissolve within the electrolyte solution, which may lead to serious secondary pollution and other issues.

Transition metal carbides (TMC, such as MXene) and transition metal dichalcogenides (TMDs) have unique two-dimensional nanostructures and excellent electrical conductivity. Researchers have carried out extensive explorations for its applications in catalysts, solar cells, secondary batteries, and capacitors [98–101]. Since two-dimensional intercalation materials such as MXene have adsorption capacity for both cations and anions [102,103], they can be introduced into CDI cells as two parallel cathodes and anodes, respectively. Srimuk et al. using a Ti_3C_2–MXene electrode constructed an HCDI system whose desalination capacity was stably maintained at 13 ± 2 mg^{-1} [58]. Since Ti_3C_2–MXene has an intercalation layered structure, its desalination mechanism is mainly ion intercalation rather than EDL adsorption. However, due to the abundant negatively charged functional groups on the surface of MXene nanosheets, its adsorption capacity for Na^+ is strong [58,102], but its removal capacity for Cl^- is significantly lower. Therefore, the application of MXene as a CDI anode requires further functional groups and structural design.

3.2. Electrode Material Design

The adsorption capacity of electrode materials plays a crucial role in the desalination performance of CDI systems. According to the capture mechanism of the CDI systems, the electrode materials may be divided into three types: electrosorption electrodes, insertion electrodes, and redox reaction electrodes. Among them, electrosorption mainly occurs on carbon electrodes, while the other two types require the introduction of Faraday electrodes. This section takes several typical examples to briefly introduce the latest research progress of carbon-based electrode materials, intercalation electrode materials, and polymerized electrode materials in the field of CDI, as well as summarizes the general strategies for electrode material optimization.

3.2.1. Carbon Material

Carbon materials have the characteristics of rich pore structure and good electrical conductivity, representing the earliest electrode materials for CDI systems. Traditional carbon materials (such as activated carbon and carbon cloth) only have a porous structure, and the removal of ions is usually achieved by an electrosorption mechanism in the CDI system. Nanostructured carbon materials (such as graphene and carbon nanomaterials) have the characteristics of intercalation materials, and the design and optimization of related materials have become the recent research emphasis.

As a common carbon-based material, carbon cloth has the characteristics of high electrical conductivity, high porousness, convenient form adjustment, and sensible mechanical stability, and it has been widely utilized in numerous fields [104]. There have been many reports on pure carbon cloth as CDI electrodes [105–107]. However, in order to further improve the energy efficiency and desalination efficiency of the CDI system, it is necessary to modify the carbon cloth surface with nanostructures. Guo et al. used a simple method to grow nitrogen-doped carbon-coated $Li_4Ti_5O_{12}$ nanosheet arrays on the surface of carbon cloth through polymerization and annealing steps [108]. Due to the Faraday effect of $Li_4Ti_5O_{12}$, the SACs of the modified electrode are increased by 300% (25 $mg{\cdot}g^{-1}$/7 $mg{\cdot}g^{-1}$) compared with the bare carbon cloth electrode. The charge efficiency is increased to 83%, the energy consumption is reduced to 9.92×10^{-20} $J{\cdot}mol^{-1}$ for ion removal, and the long-term stability exceeds 30 cycles.

As one of the most typical carbon-based nanomaterials, graphene has a honeycomb-like carbon atomic single-layer structure and a huge specific surface area (2675 $m^2{\cdot}g^{-1}$), which can be used for ion storage. The sp^2-hybridized carbon–carbon conjugated structure makes it have good electrical conductivity; hence, it is an ideal electrode material for the development of new CDI systems [109–112]. However, due to the stacking tendency of the two-dimensional structure, there is an effect on the precise expanse and effective surface adsorption capability of the electrode. Furthermore, the preparation process usually has

problems such as high material cost, introduction of toxic chemical reagents, and harsh preparation conditions, which further limits its large-scale application in CDI systems. In response to the above problems, researchers have carried out many attempts in the preparation and optimization of graphene. Using CO_2 as the raw material, metallic Mg powder as a reducing agent, and nano-magnesium oxide as a template agent, Li et al. prepared high-quality graphene rich in mesoporous structure (13,000 $S \cdot m^{-1}$, 709 $m^2 \cdot g^{-1}$) in batches under high-temperature conditions [113]. The capacitance and energy densities were 224 $F \cdot g^{-1}$ and 136 $Wh \cdot kg^{-1}$, respectively. Due to the simple preparation method and the excellent properties of the prepared porous graphene, it has great commercialization prospects.

Since graphene has fewer surface functional groups and strong π–π interactions between its layers [114,115], functional group modification is a commonly used method for stacking inhibition of nanosheets. Liu et al. used pyridine as an intercalator and dispersant agent for exfoliation and reduction of graphite oxide (Figure 4a) [110]. The π–π stacking between the pyridine benzene ring embedded into the plane of graphite oxide, which effectively suppresses the re-stacking of graphene during the reaction process, and the material exhibits good CDI performance. In addition, the introduction of other active materials between the nanosheet layers can also play a role in suppressing the stacking of nanosheets. Huang et al. added an etchant (H_2O_2) into the graphene oxide solution, and the prepared three-dimensional nanoporous structure graphene material was used as the symmetrical electrode of the CDI system. The nanopores created by the hydrothermal reaction increase the effective active surface area on the graphene nanosheets, facilitating the diffusion of ions [116].

Carbon nanotubes (CNTs) are one-dimensional tubular carbon nanomaterials with glorious electrical conductivity, appropriate pore structure, high theoretical specific surface area, and sensible mechanical stability, which are suitable for use as CDI electrodes [117,118]. However, the CNTs are inherently hydrophobic, which affects the effective contact area between the electrolyte and the electrode. Furthermore, the one-dimensional nanostructure has a tendency to aggregate, which also affects its theoretical performance [119]. Therefore, CNTs are mainly used in the form of composite materials when applied as CDI electrodes, and they are usually modified with functional groups to achieve functionalization. For example, CNTs can be used as an additive to graphene electrodes, which can prevent the aggregation of graphene nanosheets, improve electrode conductivity, and ultimately improve electrode efficiency [120].

In a recent study by Sriramulu et al., self-supporting electrode films with a layered structure were obtained by vacuum filtration of graphene oxide and two composite precursor solutions (Figure 4c) [121]. Through the reduction reaction, graphene oxide is converted into reduced graphene oxide (rGO), which improves the conductivity of the electrode. A novel high-efficiency HCDI system was constructed with the prepared self-supporting $Na_2Ti_3O_7$–CNT@reduced graphene oxide (NCNT@rGO) film as the anode and activated carbon@graphene oxide (AC@rGO) film as the cathode. In the constant-current (CC) operation mode, sodium ions are inserted into the negative electrode (NCNT@rGO), while chloride ions are adsorbed to the positive electrode surface (AC@rGO). In addition to graphene, CNTs can also be combined with a variety of materials to prepare composite materials. The unique morphological structure of one-dimensional CNTs can be used as a nano-skeleton, which enables the assembled composite materials to gain a unique three-dimensional structure. Li et al. prepared carbon nanotubes and carbon nanofibers (CNTs–CNFs) composite films with an excellent network structure as MCDI electrodes using chemical vapor deposition method (Figure 4b), which improves the desalination performance of the electrode [122].

Pan et al. explored hierarchical porous carbon nanotube (CNT)/porous carbon polyhedron (PCP) composites (hCNT/PCP) for the first time via in situ intercalation of CNTs in ZIF-8 followed by pyrolysis [123]. Due to the porous structure, high specific surface area, and good electrical conduction of the composite, hCNT/PCP exhibited a high electrosorption capability of 20.5 $mg \cdot g^{-1}$ and stable cycling stability (no significant decrease in

30 charge/discharge experiments) beneath 1.2 V operative voltage. In addition, composites of metal–organic framework (MOF)-derived carbon and carbon nanotube have controllable morphologies, appropriate pore size distribution, and wonderful electrical conductivity, which have additionally been tried to exhibit excellent desalination performance in recent studies [124]. Gao et al. grew CNTs on ZIF-67 using chemical vapor deposition, and the obtained composites were carbonized to form carbon polyhedra and carbon nanotube hybrids (HCNs) [125]. HCN features a distinctive network structure in which polyhedral porous carbons are tightly connected by ultralong carbon nanotubes (Figure 4d). HCN combines the benefits of the two materials and makes up for their shortcomings. It is an excellent electrode material with high specific surface area, sturdy hydrophilicity, and sensible electronic conduction.

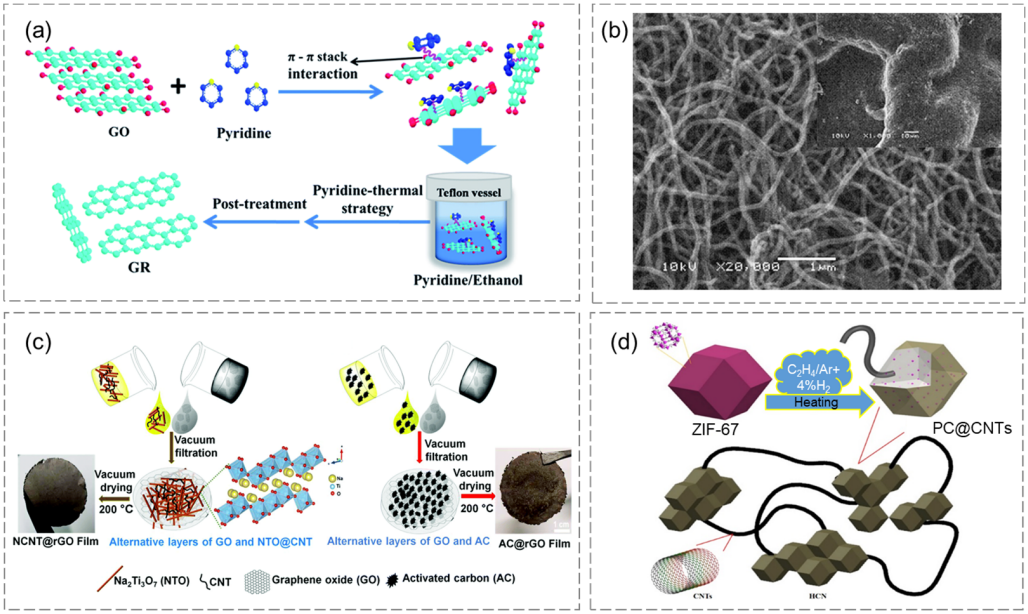


Figure 4. (**a**) The process of pyridine thermal preparation of graphene. Adapted with permission from Ref. [109]. 2017, Liu P; (**b**) SEM image of carbon nanotube and carbon nanofiber (CNT–CNF) composite film (the inset is a low magnification electron microscope image). Adapted with permission from Ref. [122]. 2008, Li H; (**c**) schematic diagram of the formation of layered NCNT@rGO films, lattice structure of $Na_2Ti_3O_7$ nanowires, and schematic illustration of AC@rGO membrane formation by vacuum infiltration of hydrophilic membranes using suspensions. Adapted with permission from Ref. [121]. 2019, Sriramulu D; (**d**) hybrid carbon nanotube (HCN) synthesis process. Adapted with permission from Ref. [125]. 2018, Gao T.

3.2.2. Insertion Electrode Materials

Cations or anions are inserted into the lattice or between sheets of electrode materials when CDI desalination is performed under the insertion mechanism. This calls for an electrode material [27,103] with a high electrical conduction, water wettability, pseudocapacitive ion storage, and straightforward ion insertion/deintercalation [126,127]. The research of related materials in the CDI desalination field has gained increasing attention. The spacious interstitial sites of electrode material led to larger ion adsorption capacities, faster adsorption kinetics, and higher cycling stability. The insertion electrode materials that have been reported for CDI systems include Prussian blue (PB) and its gels (PBAs) [128–130], MXenes [131,132], $NaFe_2P_2O_7$ [133], and $NaTi_2(PO_4)_3$ [58,134,135]. Since the charge storage mechanism of insertion materials is different from that of electrosorption materials with a pore structure, which can achieve higher storage capacity with a lower surface area.

In 2011, Gogotsi et al. first discovered a new class of two-dimensional (2D) transition metal carbon/nitrides, referred to as MXenes [136]. It has an open-layered structure, high volume capacitance, good hydrophilicity and conductivity, and tunable thickness

and interlayer spacing. An efficient ion transport path can be constructed by structural modifications, and it can achieve optimized CDI desalination performance. Agartan et al. selectively etched the MAX phase of Ti_3AlC_2 in 30% HF aqueous solution and rolled the slurry into a freestanding electrode with a thickness of about 140 µm [127]. The as-prepared $Ti_3C_2T_x$–MXene-based electrode was used in the MCDI system. Under the optimized operating conditions, the maximum SAC was 8.88 $mg \cdot g^{-1}$, and the charging efficiency was 74.47%, which was far superior to the CDI system based on carbon electrodes. Similar to 2D graphene nanosheets, the designed and modified MXene-based electrode materials can exhibit high-efficiency desalination capabilities. However, the inherent low ion diffusion characteristics of the 2D nanosheet structure limit its desalination rate, which slows down the ion diffusion rate [137]. To solve this problem, Ding et al. prepared $Ti_3C_2T_x$–MXene nanosheets using a selective etching method, which were then treated with melamine nitridation to convert MXenes into a novel nitrogen-doped three-dimensional (3D) nanofibrous structure (N-TNF) [138]. The synthesis process is shown in Figure 5a. N-TNF has a unique nanofibrous structure and abundant nitrogen-containing functional groups, which endow it with enlarged interlayer spacing, high specific surface area, and excellent electrochemical activity. N-TNF exhibits an ultrahigh average desalination rate of 5.6 $mg \cdot g^{-1} \cdot min^{-1}$, an excellent desalination capacity of 44.8 $mg \cdot g^{-1}$, and good long-term cycling stability in HCDI system, outperforming most 2D materials.

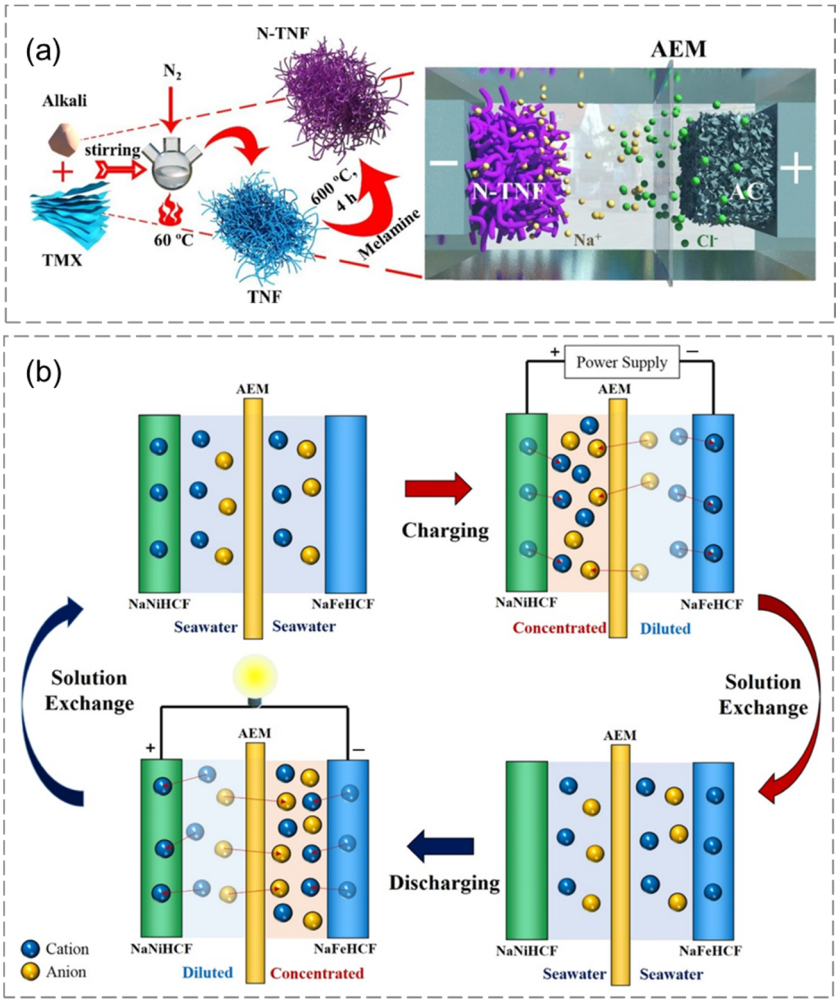


Figure 5. (**a**) Schematic diagram of N-TNF synthesis process and HCDI cell structure. Adapted with permission from Ref. [137]. 2018, Guo L; (**b**) principle of rocking-chair desalination battery based on PB material. Adapted with permission from Ref. [128]. 2017, Lee J.

In addition to the ultrahigh ion adsorption capacity, the inherent selective properties of insertion electrode materials for ions are also worthy of further research [139]. In some materials such as PBAs, the intercalation process of ions is accompanied by redox in the lattice. The mechanism excluding the co-ion repulsion during desalination [140], and the charge efficiency of the HCDI system can be effectively improved without the use of IEM [94]. PB and PBAs are a class of coordination compounds with cubic lattice structure and rich functional group, possessing an open three-dimensional (3D) framework to store cations [141]. These lattices can differentiate cations based on factors such as ion size or hydration energy, enabling the constructed CDI system to have the ability of ion selectivity [142]. Reversible insertion/de-insertion of cations in the lattice can be achieved by reacting with redox-active elements in the lattice (usually Fe^{2+}/Fe^{3+} redox pairs) [143]. The insertion/de-insertion process generally has high Coulombic efficiency, indicating that these insertion electrode materials are easy to regenerate. Lee et al. developed a rocking-chair desalination without Cl^- storage electrode based on PB material consisting of NaNiHCF and NaFeHCF electrodes (Figure 5b) [128]. During the charging process, cations in the cathodic chamber are captured by the cathodic electrode, while cations inserted into the anode are released into the anodic chamber. Real seawater electrolyte coexistence of multiple ions is used as the feed stream, and the system produces a high desalination capacity of 59.9 $mg \cdot g^{-1}$ and good stability (retaining 91.5% of the initial capacity after 100 cycles). The system can not only improve the desalination capacity, but also improve energy efficiency.

In addition to PB and its analogs, other intercalation materials such as $NaMnO_2$ (NMO), and TiS_2 have been used in CDI to selectively separate specific ions from ionic mixtures. Yoon et al. used NMO as a Na^+-selective electrode and PB as a K^+-selective electrode in an asymmetric CDI device for purification of Na-ion-contaminated KCl feed solution [37]. The results showed that, when PB is intercalated with K^+, the NMO electrode can remove 36% of Na^+ impurities in the feed solution. Kim et al. also used the λ-MnO_2/AC system to recover Li^+ from brines containing Na^+, K^+, Ca^{2+}, and Mg^{2+}, and the selectivity was due to the ease of Li^+ insertion into the λ-MnO_2 spinel structure [144]. Unlike PBAs, λ-MnO_2 mainly inserts Li^+ into other cations, and the property is attributed to the tiniest size of Li^+ ions, which inserts the lattice site of λ-MnO_2 electrodes.

3.2.3. Polymer Electrode Materials

Conductive polymer (including polyaniline (PANI) and polypyrrole (PPy))-based electrodes have been widely used in batteries and supercapacitors [145–148]. Due to the flexible preparation method and good capacitance storage capacity, they have great application potential in CDI electrode materials [149,150]. The charging or discharging process under electric field can affect specific interactions, thereby leading to the ion selectivity of electrodes. To promote the performance of conductive polymers in CDI systems, the ion–electrode interaction can be regulated through material surface design. The ion removal efficiency can be promoted by improving the conductivity of the electrode or modifying functional groups, while the selectivity of the electrode can be achieved by specific modification [151]. Selective capture of electrode is not limited to charged species; by introducing redox-active molecules or exploiting the characters of polymers, the interaction of neutral species to electrodes can be reversibly switched through electric field.

As shown in Figure 6a, PANI is composed of repeating units of phenylenediamine and quinonediamine. It is a conductive polymer with good conductivity, easy synthesis, and high pseudocapacitance [150]. When it is used as a supercapacitor electrode material, it is usually doped with selenite [152], graphene oxide [153], or hydrochloric acid [154]. Liu et al. directly electrodeposited polyoxometalates (POM) and PANI on 3D exfoliated graphite support (EGC), and the obtained composite electrode was applied in the MCDI system [155]. The composite electrode material performs high ionic capacitance and good stability. Lai et al. discovered a significant increase in capacitance after adding PANI to graphene [156]. In addition, single-walled carbon nanotubes (SWCNTs) and PANI

composites were investigated as electrode materials for CDI. The introduction of PANI modified the mesoporous structure of SWCNTs, which promoted the entry and exit of ions on the electrode surface [157]. The constructed CDI system exhibited great regeneration characteristics and improved stability, which proved the enhancement effect of PANI on the capacitance of the carbon material [158].

As a typical conductive polymer, PPy (Figure 6b) has attracted much attention due to its unique redox properties, biocompatibility, good electrical conductivity, and chemical stability [159–161]. Surfactant-functionalized conductive PPy has a special electronic configuration, which can realize the reversible adsorption and release of neutral compounds through electric field conversion [162]. However, its amorphous structure and insolubility limit further study of its structure and properties at the atomic level. Using an ab initio method, John et al. constructed the molecular mechanical fields of PPy and its derivatives [159]. The model was integrated into the optimized potentials for liquid (OPLS) force field to simulate the molecular dynamics (MD) of polypyrrole, and the structure, charge distribution, and main chain flexibility of polypyrrole were studied. The study provided a suitable fixed charge force field and facilitated the investigation of the properties of PPy and its interaction with other molecules, thus promoting the application of PPy in the field of CDI as a desirable material with inherent selectivity. Some polymer electrodes are reported to have superior electrochemical performance to carbon materials due to their all-porous structure, short diffusion paths, and large functional effective surface area. Feige et al. proved the enhancement of the overall electrosorption capacity through the use of polymer-treated electrodes [163]. The electrode had an appropriate diffusion length, large surface area, and high pore volume, presenting high SAC and high processing efficiency. To improve the utilization of a single conductive polymer material for energy storage, Ezika et al. composited conductive MXene with PPy to obtain a hybrid multifunctional material with enhanced electrochemical performance [164].

Organometallic redox polymers exhibit superior performance in controllable surface electrosorption [151]. For example, polyvinylferrocene (PVFc) has a robust structure that can be utilized to manage charge-transfer interactions with many target anions, together with organic anions and transition metal oxyanions (Figure 6c). The interaction between ferrocene units and numerous anions is widely utilized in the field of sensing. PVFc-coated electrodes have a strong affinity for carboxylates, sulfonates, and phosphates [165]. When anions are bound to electrodes, redox-active polymers can suppress side reactions and selectively capture trace amounts of micropollutants [166]. PVFc-based electrodes have been used for the capture of heavy metal oxyanions (Figure 6d). For many polymers with redox activity, the binding process can be enhanced by understanding the mechanism of ionic interactions.

The polymer precursors have extremely tunable structures, and the polymer-derived carbon materials have higher charge storage and capacitive properties. Their porosity and surface area are simply and effectively controlled by synthesis conditions. Conductive polymers are ideal electrode materials for CDI systems due to their excellent properties such as high conduction, versatility, low-cost and facile synthesis methods, higher electric double-layer capacity, and longer cycle life.

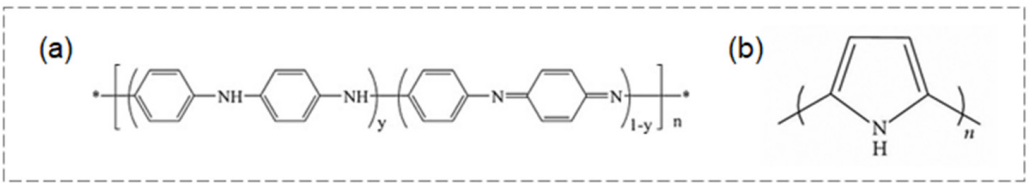


Figure 6. *Cont.*

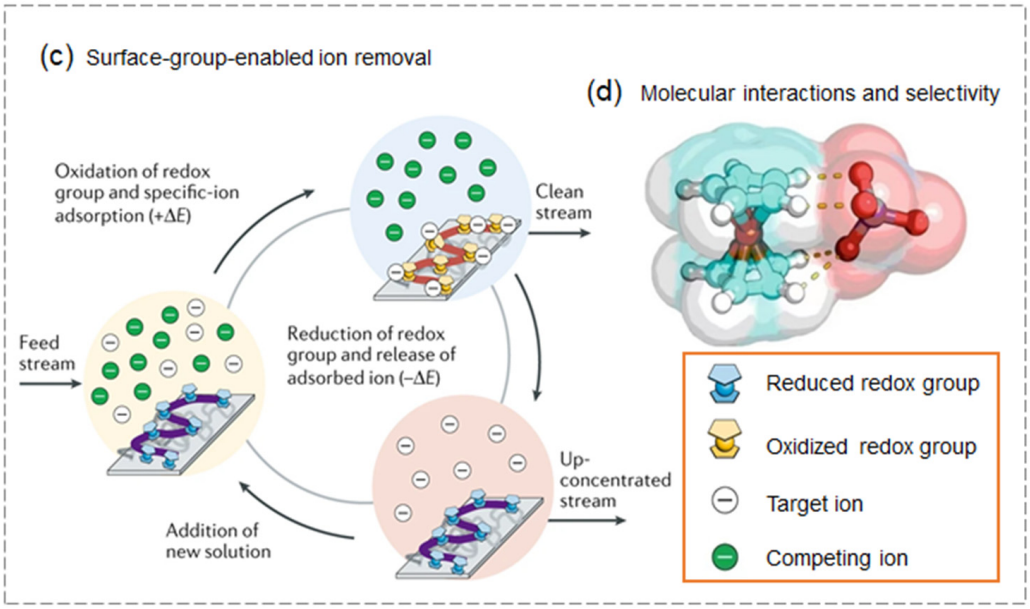


Figure 6. (**a**) Chemical structure of intrinsic polyaniline, where y is between 0 and 1, n is an integer, and * is repeating units. Adapted with permission from Ref. [145]. 2011, Zhang H; (**b**) polypyrrole chemical structure; (**c**) selective removal of ions through reversible electrochemical reactions of tailored surface groups, where ΔE is the amount of change in the electrode [151,165]; (**d**) polyvinylferrocene (PVFc) has good selectivity for various anions and can strongly bind electron-donating groups such as oxyanions. Adapted with permission from Ref. [167]. 2018, Su X.

3.2.4. Fibrous Membranes Materials

Recent studies have shown that fibrous membranes prepared by electrospinning methods often have high porosity, high specific surface area, and easily adjustable structures. Electrospinning is one of the most prevalent methods for producing free-standing nanofiber electrodes using polymer precursors. This method has been attractive to many researchers regarding its tunable and favorable properties. Typically, electrospinning is a fiber production method in which the charged precursor solution (as an anode) is spread to an oppositely charged substrate or rotating drums (as a cathode) [131].

In a study by Ding et al., a free-standing polymer/MOF composite electrode was fabricated using the electrospinning method followed by an annealing process leading to a satisfactory capacity. Carbon nanofibers encased the MOF-derived carbon nanoparticles, which led to higher electrical conductivity and prevented aggregation [168]. Another desalination study was carried out by Liu et al. using electrospun CNF- and MOF-derived porous carbon polyhedral (PCP), followed by thermal treatment, to produce a freestanding CDI electrode which outperformed its counterparts in other CDI devices [169]. In order to improve the electrochemical performance, specific capacitance, and pore structure of electrodes, some researchers have suggested the growth of metal oxides on CNF substrates as a promising and fruitful way to improve the electroadsorption function of electrodes. Among them, the desalting performance of self-supporting electrospun NiO-doped porous carbon nanofiber electrodes was evaluated by Hussain et al. [170]. Due to sufficient micropores, mesopores, and macropores, the addition of an appropriate amount of NiO to carbon nanofibers can improve the hydrophilicity, electrochemical performance, and double-layer capacitance. Since electrode conductivity is one of the most important factors in the CDI process, increasing this parameter can potentially lead to more fruitful results. Wang et al. prepared rGO/activated carbon fiber (ACF)-composite independent electrodes for CDI using polymer-based cornerstone ink composite precursors with different RGO-to-polyacrylonitrile ratios by electrospinning and then heating activation. The addition of more conductive material to the electrospinning precursor greatly enhances the ability of the electrode in terms of conductivity and ion storage. The inclusion of graphene in the

net structure of ACF enables the electrode to have a good porous structure and electrical conductivity, as well as a high electroadsorption performance [171].

In conclusion, there is still much room for the development of freestanding electrodes with excellent robustness and mechanical stability, high conductivity, large-scale manufacturing capability, and super-strong ion removal capability. In addition, these substrates must provide a high-loading platform for nanoparticles with good redox activity. The electrospinning method can be used to construct a micro/nano permeable and porous interface structure. It is a good method to improve the wettability of electrode and reduce the resistance of ion transport, which is helpful to improve the electroadsorption efficiency of CDI electrode to remove ionic pollutants.

3.3. Operation Mode

The operation process of CDI technology can be divided into the electro-adsorption of salt ions on the porous electrode (also called the "charging" stage) and the electrodesorption (also called the "discharging" stage) process, which are alternately cycled. Among them, the electro-adsorption process can be divided into two operation modes: constant-voltage adsorption (CVA) [172,173] and constant-current adsorption (CCA) [174–176] according to the applied electric energy. In order to prevent the energy consumption caused by the Faradaic reaction, the electro-adsorption process CDI is usually performed under a low charging voltage [177]. However, applying a higher charging voltage to the CDI cell can effectively improve the ion adsorption capacity according to the EDL model. Therefore, the selection of a suitable operating voltage is crucial for the improvement of the salt removal performance of the CDI system. Compared with the CVA mode, the electrode is exposed to the high-voltage condition for a shorter time under the CCA mode, which results in a lower internal resistance value and lower parasitic energy loss of the system [178]. Hence, the CCA mode is more advantageous than the CVA mode. The energy consumed during the charging process can be stored inside the electrode. Lin et al. investigated the effect of different charging modes on energy recovery and electrode regeneration [179]. Figure 7a,b show that the energy recovery of the MCDI system decreased with the rise in charging current/voltage upon charging the MCDI system in CCA and CVA modes. The increase in discharge current also adversely affects the energy recovery rate of the system; therefore, the energy recovery rate of the CCA mode is mostly beyond the CVA mode. In addition, the electrode regeneration rate increases with the decreased discharge current, and the electrode regeneration rate in CCA mode (86%) is significantly higher than that in CVA mode (64%) under 0.1 A discharge current (Figure 7c,d).

The electrodesorption process includes three operation modes: zero-voltage desorption (ZVD) [180], reverse current desorption (RCD) [47], and reverse voltage desorption (RVD) [49]. Among them, the RVD and RCD modes can achieve effective desorption only in the presence of IEMs; hence, they are not suitable for the traditional CDI system. The most used operation mode of the CDI system is CVA/ZVD. Figure 7e shows the curve of effluent salt concentration with time in one operation cycle [17,18,181]. The initial desalination rate is the highest because of the initial feed stream, and then the ion concentration in the effluent rapidly decreases to the lowest value. With the increase in reverse EDL voltage, the desalination rate slows down and the effluent salt concentration slowly rises to the feed value [17]. During the ZVD process, the counter ions are spontaneously discharged from the electrode into the spacer channel until the electrode micropores are no longer charged [77]. The electrode desorption rate is the fastest when the counterion concentration in the EDLs is the largest; thus, the salt concentration during the ZVD process exhibits a narrow peak, and the desorption rate slows down when the EDLs are close to electroneutrality.

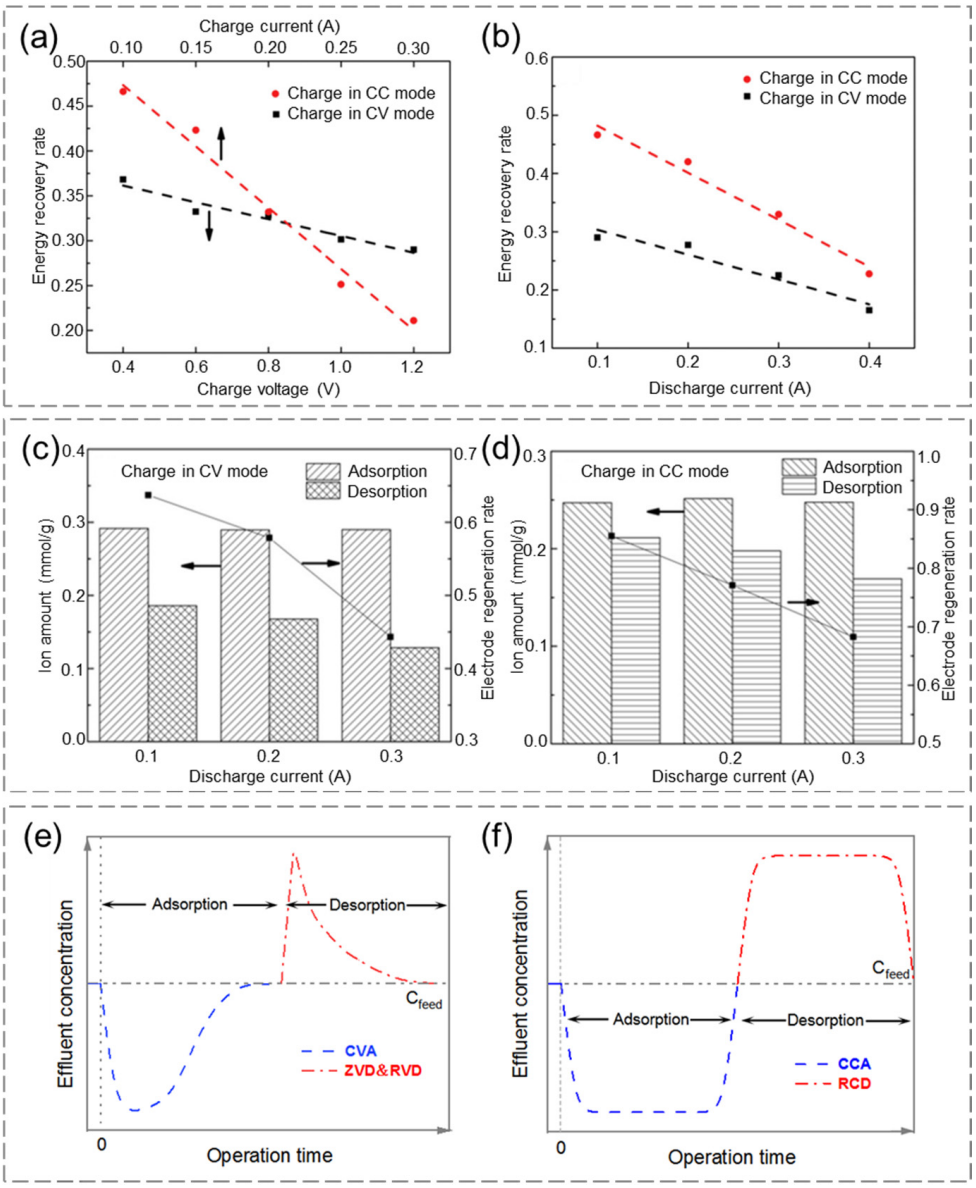


Figure 7. In CC and CV modes, the energy recovery rate of the MCDI system (**a**) under different charging and same discharge current of 0.1 A, and (**b**) under different discharge current (0.1–0.4 A). Adapted with permission from Ref. [179]. 2018, Chen L; (**c**) charge in CV mode; (**d**) adsorbed/desorbed ion amount and electrode regeneration rate of the MCDI stack in CC charging mode. Adapted with permission from Ref. [179]. 2018, Chen L; (**e**) CVA, ZVD, and RVD; (**f**) CCA and RCD dimensionless and idealized effluent salt concentration curves, where the horizontal dashed line represents the feed salt concentration. Adapted with permission from Ref. [54]. 2020, Liu E. (The up and down arrows represent coordinates of CA and CC respectively; The left arrow represents the coordinates of the ion amount and the right arrow represents the coordinates of the energy regeneration rate.).

In RVD mode, the counter ions are not only desorbed by the electrode repulsion, but also driven by the reverse electric field, which accelerates the electrode desorption rate by 30% [69]. The ions are first desorbed from the EDL in the micropore, and the co-ions act as counter ions to attract them under the action of the reverse electric field. Then, the ions are desorbed from the macropores between the electrode particles, and the salt ion concentration in the macropores drops sharply until it approaches zero at the end of the desorption process. In this way, the RVD can more effectively remove the counter ions from the electrode structure, so that the adsorption rate and capacity of the counter ions

are increased during the adsorption process of the next cycle [17]. Compared with the ZVD operating mode, the salt removal rate was increased by 20% in the RVD mode [69]. The advantage of CCA [181,182] and RCD [47,182] modes is their constant and adjustable effluent salt concentration. In CCA mode, the ionic current is determined by the counter ion adsorption flux and the co-ion expulsion flux. The introduction of IEMs effectively reduces the co-ion flux in MCDI. Therefore, the applied constant ionic current is interpreted into a constant counter ion adsorption flux, which results in a constant salt removal rate for the overall solution, and further maintains the salt concentration in the effluent constant (Figure 7f) [181]. As the effluent electrolyte concentration decreases, the reverse EDL voltage at the electrode interface increases, and the voltage needed to keep up constant current increases steadily [47]. When the voltage reaches a certain value (such as 1.2 V, 1.4 V, and 1.6 V) [176,182], the CCA stops and starts the desorption step. Similar to CCA, in the presence of IEMs, the concentrated stream produced by RCD mode has a constant concentration [17]. It has a good "purifying" effect on the electrode during the desorption process, which can alleviate the electrode and membrane fouling problems during the adsorption process. However, the fouling mitigation mechanism in the RCD process needs further research.

Since the selection of the CDI operation mode has a great influence on the performance of the system, it should be reasonably selected according to the requirements in the actual application. The "purifying" effect of the reverse desorption mode (RVD and RCD) leads to an increase in the adsorption capacity and adsorption rate in the next adsorption cycle, which is beneficial to the desalination treatment of high-concentration industrial brine. In addition, the reverse desorption mode can alleviate the electrode and membrane fouling problems in the CDI system, which is beneficial to the treatment of industrial brine with high fouling potential. However, the effectiveness and mechanism of pollution mitigation in reverse desorption mode have not been fully demonstrated. The main advantage of constant-current operation (CCA and RCD) is the constant effluent concentration. Particularly multistage operation has to be introduced facing with high-concentration brine, which may effectively simplify the operation management of the system.

3.4. Technoeconomic Evaluation

Numerous studies of CDI have focused on increasing the production capacity and energy consumption through materials (such as ion selective membranes and charged carbon) and operational improvements. However, there is a gap between laboratory-scale experimental and practical application. The capital and operating costs of the technology need further evaluation. Some performance metrics, including thermodynamic efficiency (η_T) and recently volumetric energy consumption (Ev, $W{\cdot}h{\cdot}m^{-3}$) [18], have been used to compare the direct energy footprint of CDI with other desalination technologies. On the basis of the developed performance metrics, the tradeoff and optimization strategy of CDI operation mode have been determined [48]. In these studies, it was generally considered that productivity and energy consumption are alternative metrics of capital and operating costs, respectively. However, the relationship between individual performance metrics and the estimated cost of CDI systems has been less studied.

Steven et al. developed a parameterized framework that can be used to determine the size and cost of an (M) CDI system for specific operational requirements [183]. The number of cell pairs of the system and the required quality can be calculated by inputting reported materials and operation conditions. The output can then be used to calculate capital costs (electrodes, housing/assembly, current collectors, IEMs, power, and thermal regulation costs) and operating costs (electricity costs). The framework provides a simple system cost estimate for any proposed material or operational improvement. By incorporating the uncertainty of material design, operation, and parameters, the key performance and lifetime of the (M) CDI systems can be benchmarked. However, both the capital and the operating costs are greatly reduced when treating low concentration feedwater. Therefore, CDI may be an economical alternative to membrane-based technologies such as RO when

selective ion removal in low salinity water is required. The study is limited to evaluating the size and design of the CDI system, whose influent and effluent are typical saltwater and drinking water, respectively.

Although energy consumption was an important consideration in many desalination studies, it is challenging to provide an evaluation of energy efficiency due to the different separation mechanisms achieved by the various desalination processes. Lin et al. suggested the energy efficiency of any desalination process can be quantified in terms of thermodynamic energy efficiency (TEE), which accounts for the inherent "difficulty" of the separation process [184]. Theoretically, non-thermal desalination processes are energy efficient because they direct energy to brine separation rather than inducing phase changes. However, the activated carbon electrodes CDI system stores a large amount of energy during the charging phase, which brings great challenges to achieve high TEE. The TEE of CDI can be effectively improved by reducing the excess voltage. This calls for further efforts on using high-capacitance electrodes (more AC electrode mass per unit area or electrodes made of intercalated materials) and optimizing the operation (reducing the current density and maximizing the energy recovery during discharge).

Overall, current scientific research tends to focus on technical specifications, but the energy consumption in desalination is actually only related to the overall cost of water treatment. Research into new desalination technologies should aim to achieve lower overall treatment costs, instead of just improving energy efficiency.

4. Emerging Application Fields

In addition to the widely applied seawater or industrial brine desalination, CDI can be used in some novel ion separation applications. From the environmental treatment, CDI systems can be applied to the selective removal of ionic pollutants, including applications such as drinking water softening, heavy-metal ion removal, and CO_2 capture. From the resource recovery, CDI systems can selectively separate and recover high-value ions from the water environment. Through electrode design and operation optimization, CDI technology can achieve high-efficiency recovery of anions and cations separately or even simultaneously. Furthermore, the development of the coupling system can effectively overcome the limitations of the CDI system and further expand its application fields. In this section, we summarize the coupling technology of CDI with RO, as well as photochemistry and bioelectrochemistry, and we clarify its technical advantages and applicable field of application.

4.1. Contaminant Removal

4.1.1. Water Softening

Hard water contains a variety of soluble mineral elements such as Ca^{2+} and Mg^{2+}. The existence of the hardness ions can lead to membrane fouling, pipeline blockage, scaling, and other problems. A variety of water-softening technologies have been developed to remove Ca^{2+}, Mg^{2+}, and other metal cations in hard water [185,186], including chemical precipitation [187,188], ion exchange [189], nanofiltration, and reverse osmosis membrane technology [190,191]. However, these typical technologies usually need high energy input, have high operative costs, and use chemicals that cause environmental concerns. Recent studies have shown that CDI systems can utilize the strong interaction between the Faraday electrodes and metal ions to achieve efficient softening of hard water. Compared with traditional water-softening technology, CDI technology has the advantages of less production of hard waste, no need to introduce external chemicals, and low energy consumption, which makes it a good alternative for hardness ion removal.

The mechanism of CDI for hardness ion removal is mainly based on two aspects: ionic interaction strength and ion replacement reaction. The electrostatic attraction between two charges determines the removal of hardness ions under electric field. It is proportional to the number of charges, inversely proportional to the distance between the charges, and inversely proportional to the hydration radius of the ions. Since hardness ions are usually

multivalent, CDI electrodes exhibit stronger electrostatic attraction for them compared to monovalent cations [192]. The order of attraction of different cations on the carbon electrode surface is $Ca^{2+} > K^{+} > Na^{+}$ [193]. The ion replacement reaction is the replacement of ions adsorbed on the carbon electrode by ions dissolved in the bulk solution, which is an important factor for the selective removal of hardness ions by CDI. As shown in Figure 8a, the captured Na^{+} on the CDI electrode was replaced by Ca^{2+}, indicating the stronger attraction of electrode to divalent Ca^{2+} [29]. Since Mg^{2+} and Ca^{2+} have the same number of electrons and similar hydration radii, the removal trends of the two main hardness elements in the CDI system are similar [194].

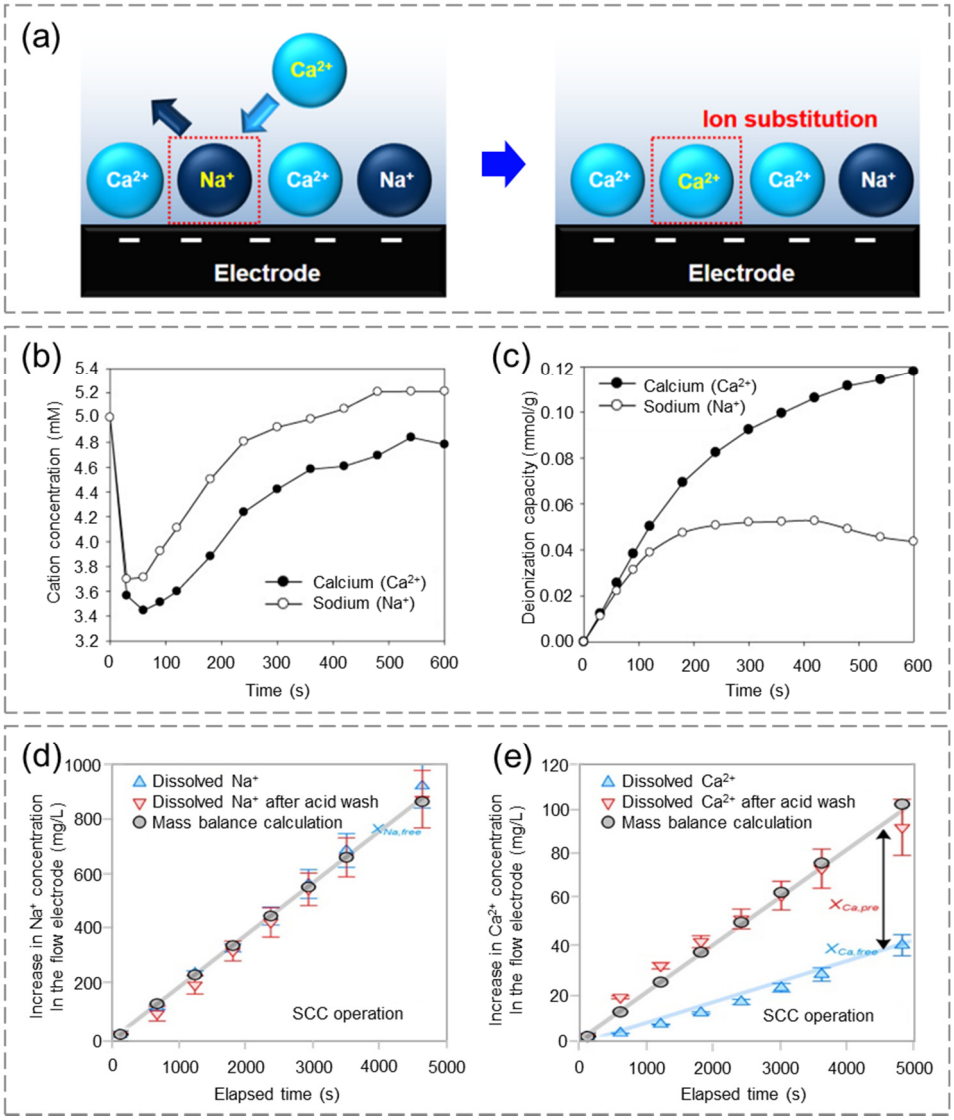


Figure 8. (**a**) Schematic illustration of the substitution effect on carbon electrodes [29,192,193]. The deionization performance of calcium-alginate-coated MCDI (CA-MCDI) is expressed as (**b**) effluent cation concentration and (**c**) selective deionization ability in 5 mM $CaCl_2$ and 5 mM NaCl mixture solution. Adapted with permission from Ref. [194]. 1996, Aslani P; (**d**) Na^{+} and (**e**) Ca^{2+} concentrations in flow electrodes in SCC operation. Adapted with permission from Ref. [84]. 2018, He C.

Using the ion replacement reaction, Yoon et al. prepared a low-cost calcium alginate coated carbon electrodes to enhance the interaction between the electrode and multivalent ions [29,194,195]. Since the calcium alginate-coated CDI electrode is more attractive to divalent cations (Ca^{2+}) than monovalent cations (Na^{+}), the constructed MCDI system has a stronger removal effect of the hardness species Ca^{2+} (Figure 8b). As shown in Figure 8c,

the removal capacity of Ca^{2+} continued to increase and did not reach a steady state after 8 min. This indicates the replacement of the Na^+ adsorbed on the electrode surface by Ca^{2+}, which was derived from the higher selectivity of MCDI system toward Ca^{2+} than Na^+. Compared with the bare carbon electrode, the calcium alginate-coated electrode assembled CDI system had a 44% increase in the removal rate of Ca^{2+}, indicating its great potential as an ecofriendly water-softening technology [29].

In addition to electrode material modification, the application of FCDI system in water softening has gradually attracted attention [20,196]. A study used FCDI to treat a feed solution containing 2000 $mg \cdot L^{-1}$ NaCl and 150 $mg \cdot L^{-1}$ $CaCl_2$. The obtained diluted water had TDS < 500 $mg \cdot L^{-1}$ and $CaCl_2$ < 15 $mg \cdot L^{-1}$, and the unit processing energy consumption was only 0.44 $kWh \cdot m^{-3}$, which proves that FCDI has great potential in water-softening applications [84]. He et al. proved that the FCDI using short circuit closed cycle (SCC) had the best water-softening effect among different cell configurations [84,192]. As shown in Figure 8d, all the dissolved Na^+ in the flow electrode was removed from the feed solution, while 60% of Ca^{2+} was fixed on the carbon particles through the membrane (Figure 8e). The system effectively alleviated the accumulation of Ca^{2+}, which can be a cost-effective method for water softening. However, this study did not consider the energy consumption of electrode and feed flow pumping, which is not adequate enough for energy recovery and cost evaluation.

At present, the research on the application of CDI for water softening remains in its infancy, and further research must be distributed to gauge its feasibility. This will lay a theoretical foundation for the sensible application and development of CDI systems in water softening. In future research, continuous attention should be paid to the development of selective electrode materials, which will improve the removal selectivity of CDI and prevent scaling [66]. For the FCDI system, the research on its long-term durability, economy, and regeneration in the process of water softening is particularly important.

4.1.2. Heavy-Metal Removal

Toxic heavy metals such as lead, cadmium, copper, arsenic, and chromium in water can cause serious environmental problems and have become a major environmental health hazard worldwide [197]. Existing heavy metal removal technologies include chemical sediment, ion exchange, adsorption, electrochemistry, and membrane-based water treatment methods. However, these traditional methods usually produce secondary byproducts, and the processing cost and energy consumption are usually high, limiting their large-scale application [30]. Recent studies have shown the feasibility of CDI in heavy-metal removal (Figure 9a). It has high energy efficiency without introducing chemicals and produces no secondary waste.

At present, CDI technology has shown excellent ion removal performance when treating arsenic [198,199], lead [200], copper [201], uranium [202], and other heavy metals. Since the CDI system can simultaneously remove anions and cations, it has obvious advantages for the removal of heavy-metal ions with various valent states. Chen et al. found that As(V) and As(III) can be removed simultaneously using CDI. The removal efficiency of arsenic ions could be improved by increasing the applied voltage and initial concentration, and the adsorption amount of As(V) was higher than that of As(III) [197]. However, when NaCl or natural organic matter (NOM) was present, the removal rates of both arsenic ions decreased due to the competitive effect. NOM may obstruct electrode pores, thereby reducing the effective specific surface area of the electrode. In contrast, the activated carbon electrode effectively removes copper even in competition with NaCl and NOM [203]. In addition, the pH of the electrolyte has a significant effect on the removal efficiency of heavy-metal ions during the removal of heavy-metal ions such as Pb^{2+} by CDI process [200]. Liu et al. studied the difference in the removal efficiency of Li^+ and Na^+ by pH. The results showed that the removal rate of Li^+ was highest when the pH was close to 6, and the removal selectivity between Li^+ and Na^+ was higher under the condition of shorter operation time and neutral pH [112]. Due to the low sensitivity of the FCDI system to the pH value of the

feed liquid, the FCDI system has a stronger technical advantage than the CDI system when dealing with Li^+ and other heavy metals that are highly dependent on pH.

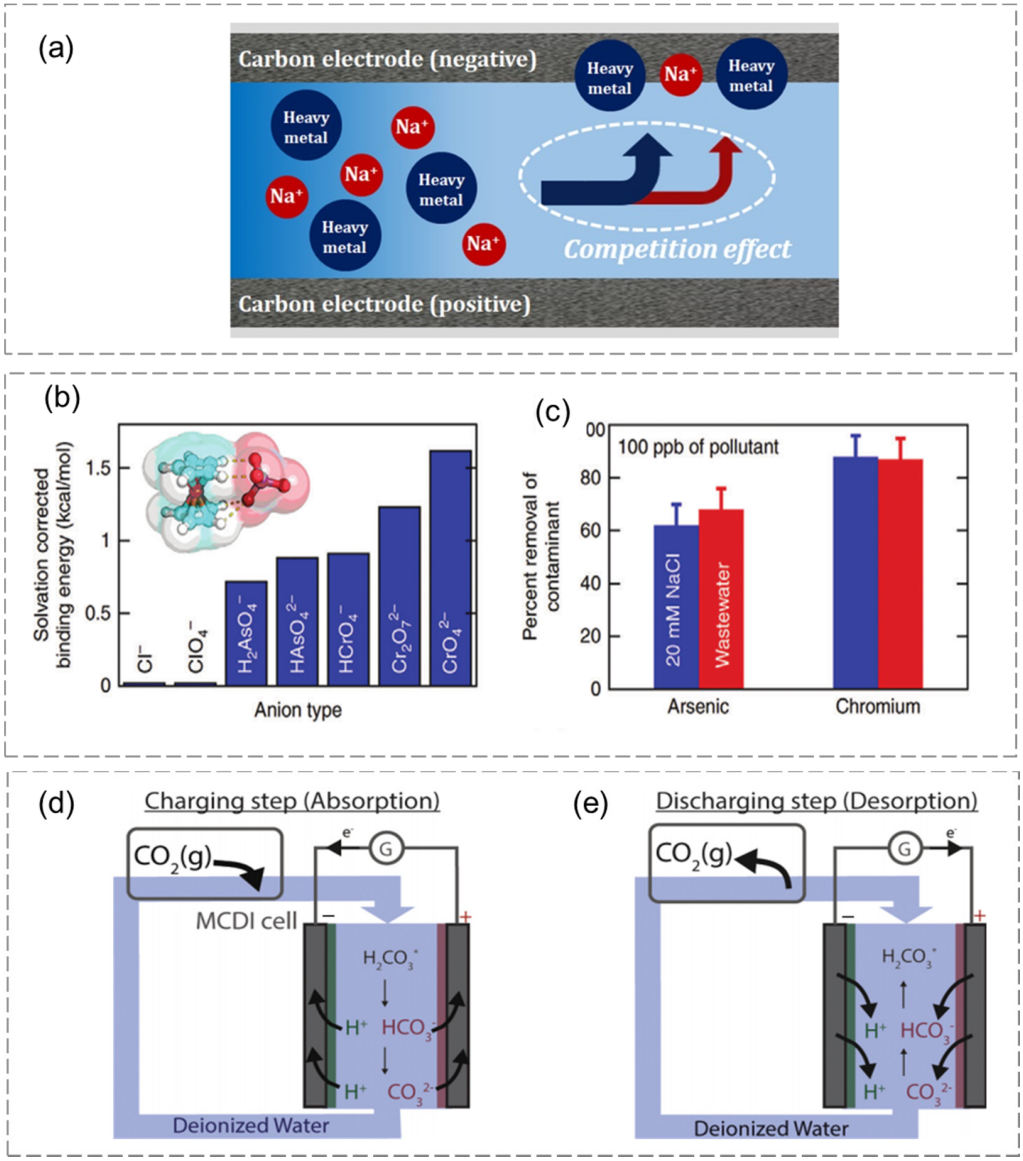


Figure 9. (**a**) Study on the mechanism of heavy metal removal by CDI. Adapted with permission from Ref. [30]. 2019, Choi J; (**b**) solvation-corrected binding energies between redox-active ferrocene and oxyanions calculated by DFT (the inset is the electronic structure optimization of CrO_4^{2-}). Adapted with permission from Ref. [167]. 2018, Su X; (**c**) the removal efficiency of chromium and arsenic under different water matrices; (**d**) schematic illustration of CO_2 capture in a CO_2-MCDI battery during charging and (**e**) discharging.

When CDI is used for heavy-metal ion removal, the selective adsorption of heavy-metal ions by CDI electrodes is a key factor determining the performance of the system. Therefore, researchers have developed a series of Faradaic electrode materials with selective functions for heavy-metal ions, including manganese oxides [73,204,205], metal hexacyanoformates [206], and polymers [170,207,208]. Li et al. prepared an α-MnO_2/carbon fiber paper (α-MnO_2/CFP) composite electrode for Ni^{2+} removal from industrial wastewater [73]. Due to the intercalation reaction of Ni^{2+} between MnO_2 crystals, accompanied by efficient charge transfer, compared with the pure CFP electrode (0.034 mg $Ni^{2+}{\cdot}g^{-1}$) and the AC electrode (2.5 mg $Ni^{2+}{\cdot}g^{-1}$), the α-MnO_2/CFP electrode exhibited higher Ni^{2+} removal capacity (16.4 mg $Ni^{2+}{\cdot}g^{-1}$). Liu et al. prepared a 2D manganese oxide/carbon nanotube

composite electrode, which had a removal capacity of 155.6 $mg \cdot g^{-1}$ and 158.4 $mg \cdot g^{-1}$ for Zn^{2+} and Ni^{2+}, respectively [203]. Since most chromium and arsenic species exist in the form of oxygen-containing anions (such as $Cr_2O_7^{2-}$, CrO_4^{2-}, $HCrO_4^-$, $H_2AsO_4^-$, and $HAsO_4^{2-}$), the development of related CDI electrode materials is also critical to their application in heavy-metal ion removal. Su et al. prepared a metal–polymer composite electrode material to selectively remove high-valence chromium and arsenic ions [167]. DFT simulation results showed that there is a good charge transfer pathway between ferrocene salt and oxyanion. As shown in Figure 9b,c, the electrode material could achieve high-efficiency removal of chromium and arsenic in both the concentration range of 20×10^{-3} M NaCl solution and actual wastewater.

Although, in recent studies, spreads of electrode materials were shown to have strong interactions with heavy-metal cations or oxygen anions, the mechanism of electrode material in trapping different ions may be different. Furthermore, the actual wastewater contains a variety of coexisting cations and anions, and the pH value fluctuates greatly, making the removal process of heavy-metal ions more complicated and difficult. Therefore, the feasibility of applying the CDI system to the removal of heavy metals still needs to be further explored.

4.1.3. CO_2 Capture

As the most common greenhouse gas, the content of CO_2 in the atmosphere is increasing year by year. Controlling the growth of CO_2 has become one of the biggest technical challenges in this century. Existing CO_2 separation and capture technologies include absorption [209,210], membrane separation [211,212], electrochemical methods [213–215], and biochemical methods [216,217]. Problems such as low energy efficiency [218–220], toxic chemical emissions [221], and corrosive effects [222] remain due to conventional technologies. As an emerging research field, the application feasibility of CDI in CO_2 capture and recovery has been confirmed [41].

Legrand et al. proposed a method for CO_2 capture based on an MCDI system [41]. In this study, MCDI technology was used to capture CO_2 in HCO_3^- and CO_3^{2-} forms. As shown in Figure 9d,e, carbonate ions (HCO_3^- and CO_3^{2-}) and H^+ are adsorbed into the electrode pores under an electric field, respectively, and stored in the electric double layer (EDL). The dissolution and ionization equilibrium of CO_2 in deionized water is replaced, which enhances the absorption of CO_2. Carbonate ions (HCO_3^- and CO_3^{2-}) can be desorbed from the carbon electrode under an applied reverse current. The chemical equilibrium correspondingly shifts to the opposite direction, which allows CO_2 to desorb into the gas phase. Therefore, by controlling the applied current and energization time, the concentration of CO_2 can be precisely controlled. The energy consumption of the system was about 40 $kJ \cdot mol^{-1}$ at a CO_2 concentration of 15%, and it could be further optimized by reducing the ohmic and non-ohmic energy losses of MCDI cells. The method can capture CO_2 at room temperature and normal pressure without using chemicals, and it has good potential in the application of CO_2 capture and recovery. Shu et al. compared the CO_2 uptake effect of three CDI systems with double membrane (CO_2-MCDI), single membrane (AEM or CEM), and no membrane (CO_2-CDI) [40], so as to explore the role of electrodes and IEMs of MCDI system in CO_2 capture application. The results showed that AEM was critical for maintaining high CO_2 absorption efficiency, while CO_2-CDI cells had lower absorption efficiency than expected.

At present, researchers have proposed a new concept of CO_2 capture using CDI electrodes and deionized water. Existing research shows that MCDI can be used to capture carbonate ions (HCO_3^- and CO_3^{2-}) produced by the reaction of CO_2 with water. The MCDI system can capture CO_2 with low energy consumption without using any chemical solvent and external heating source. During this process, the adsorption and desorption equilibrium of carbonate ions (HCO_3^- and CO_3^{2-}) in deionized water drives the adsorption/desorption equilibrium of CO_2 in the gas phase. In future studies, general evaluation methods should be developed to compare MCDI with other CO_2 capture technologies.

4.2. Resource Recovery

4.2.1. Lithium Extraction

Lithium is the third element in the periodic table and has a wide range of applications in the fields of energy, medicine, aerospace, and other industries due to its unique chemical properties [223,224]. Therefore, there is an urgent need to develop efficient lithium recovery methods to meet the substantially increasing lithium consumption demand. The lithium content in brine, salt lakes, and other water resources is as high as nearly 25 million tons, accounting for 62% of global lithium reserves [225–227]. Currently, the foremost usually used technique for lithium extraction is the lime–soda evaporation method, which is not only time-consuming, but also greatly affected by weather conditions [228]. In addition, due to the existence of a variety of coexisting ions in the concentrated solution [203], the subsequent precipitation method removes divalent cations, leading to a large amount of sludge [33]. Recently, electrochemical lithium recovery has gradually emerged as a potential alternative for lithium extraction from lithium-containing solutions thanks to its high efficiency, selectivity, and low energy consumption [229–232].

The electrochemical lithium recovery emphasizes the separation of Li^+ from other cations in the salt solution (ion selectivity) [233]. Therefore, a Faraday electrode that can selectively capture Li^+ is usually required. Compared with evaporative lithium extraction, the electrochemical lithium recovery technology can significantly shorten the treatment time, and subsequent precipitation steps are not required to remove divalent ions. Figure 10a–d are schematic diagrams of several typical electrochemical lithium recovery reaction devices based on Li^+-selective electrodes. Figure 10a shows the device with a porous carbon electrode attached to an AEM as the cathode. During the lithium ion adsorption stage, the cathode selectively captures Li^+ from the electrolyte, while only Cl^- is captured at the carbon anode [146,234]. After several cycles of adsorption and desorption operation, the concentration of Li^+ within the electrolyte decreased significantly whereas the concentrations of other cations remain virtually unchanged. Due to the highly targeted reaction, the reactor enables efficient lithium ion recovery with low energy input.

In addition, researchers have developed PPy electrodes that can undergo pseudocapacitive reactions with anions in aqueous solutions and replace IEMs. The assembled reaction device still showed strong stability after 200 cycles (Figure 10b) [235,236]. As shown in Figure 10c, Liu et al. developed a Faraday reaction system with a rocking-chair structure. The AEM divides the electrochemical reactor into two chambers, one for the lithium-containing salt solution and the other for the recovery solution ($FePO_4$ and $LiFePO_4$ in the brine and recovery solution, respectively) [237,238]. Two symmetrical electrodes are placed in the two chambers, and the Li^+ content in the electrodes varies with the reaction process ($LiFePO_4$ and $FePO_4$). The recovery of lithium ions can also be achieved by the replacement of other ions in the electrode. Using $Na_{0.44}MnO_2$ [31] and KNiFe(CN) [32] electrodes with Li^+-repelling properties as anodes, a heterogeneous Faraday electrochemical reactor was constructed (Figure 10d). After the reaction starts, the Li^+ selective electrode captures Li^+ at the cathode, while Na^+ or K^+ is released from the Li^+ repelling electrode. Then Na^+ or K^+ is trapped on the Li^+ repelling electrode and completes the electrode regeneration, while Li^+ is released from the Li^+ selective electrode into the recovery solution. The system exhibits high selectivity and high energy efficiency.

As the core element of electrochemical lithium recovery technology, the adsorption activity of Li^+ selective electrode is the decisive factor for system performance. The first study of MCDI applied to lithium separation was to coat lithium-selective materials (such as $LiMn_2O$) on activated carbon electrodes [239]. The results showed that Li–Mn–O compounds are a class of highly selective lithium-adsorbing electrode materials. Zhang et al. proved that lithium titanium oxide (LTO) spinel is also an ideal electrode material for electrochemical lithium recovery systems [240,241]. In addition to the selective electrode for efficient Li^+ capture, the ion desorption process plays a crucial role in the performance of the system. Anna Siekierka et al. proposed an HCDI system with fast adsorption and desorption properties [242]. The cathode was composed of spinel-type Li^+ selective elec-

trode material, and the anode was composed of AEM and activated carbon electrodes. The system could effectively selectively recover lithium from geothermal brine [32], and the Na:K:Li ratio in the recovery solution could be reduced from 227:1:1.1 to 2.9:0:1 in one cycle [243]. In addition, the research group also improved the preparation process of Li–Mn–Ti–O compounds. Since the Li–Mn–O and Li–Ti–O structures are the basis for the Li^+ selective electrodes, the study compared the optimization schemes of Li/Mn/Ti adsorption electrode structures with different ratios. An HCDI cathode suitable for lithium extraction from multicomponent geothermal water was constructed. Therefore, the idea of using electrochemical lithium recovery method to separate Li^+ from aqueous solution is feasible and has a relatively broad development space.

In addition to the recovery of lithium using the cathode of CDI, the synchronous recovery of anions and cations can be achieved through electrode design. Wei et al. developed a new CDI system that can simultaneously and accurately extract Li^+ and $B(OH)_4^-$ ions from salt-lake brine with high Mg/Li ratio [244]. The adsorption and desorption processes are shown in Figure 10e. The oxygen vacancy-rich $CoP/Co_3O_4^-$ graphene aerogel ($GA/CoP/Co_3O_4$) bifunctional electrode was used as the positive and negative electrode of the system. When the ratio of Mg/Li in the feed solution was 24:1 and the ratio of Cl/B was 70:1, the effective adsorption amounts of Li^+ and $B(OH)_4^-$ ions reached 37 $mg \cdot g^{-1}$ and 70 $mg \cdot g^{-1}$, respectively. The CDI system had good electrochemical adsorption/desorption stability, and the recovery rate could reach 90% after 10 cycles. Although a series of studies have focused on improving the economic feasibility and lithium recovery performance of CDI systems, the comparison of the performance is not clear due to the various performance parameters and experimental conditions of the current research. In addition to continuing to focus on improving lithium recovery performance, reducing energy consumption, investigating novel Li^+ selective electrode materials, and optimizing system configuration, researchers need to develop a standardized method to evaluate the performance of electrochemical lithium recovery systems, which will allow for more accurate performance comparisons, and further advance the field.

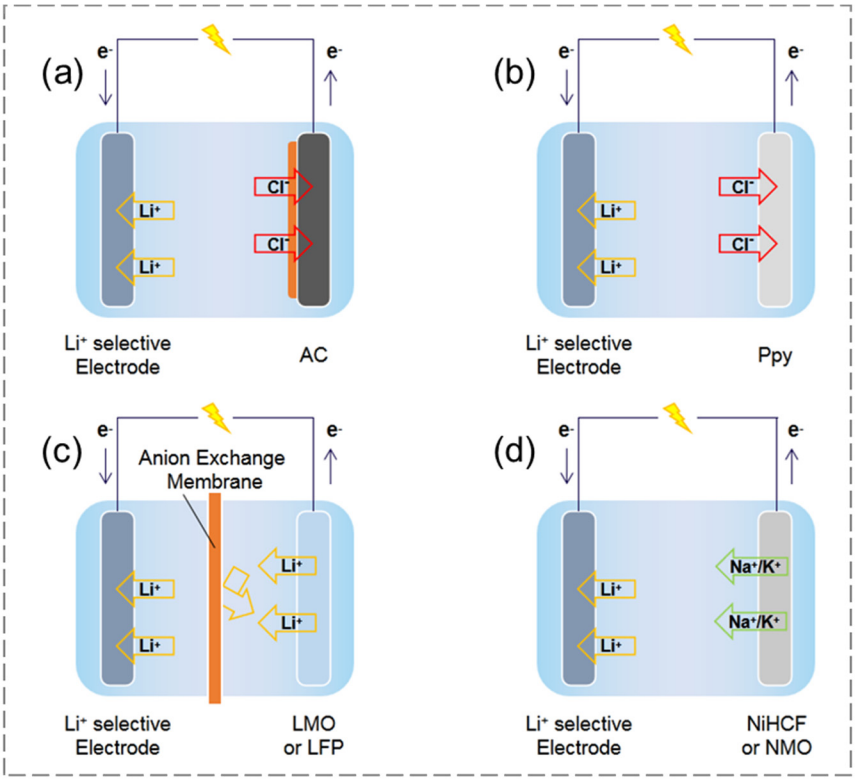


Figure 10. *Cont.*

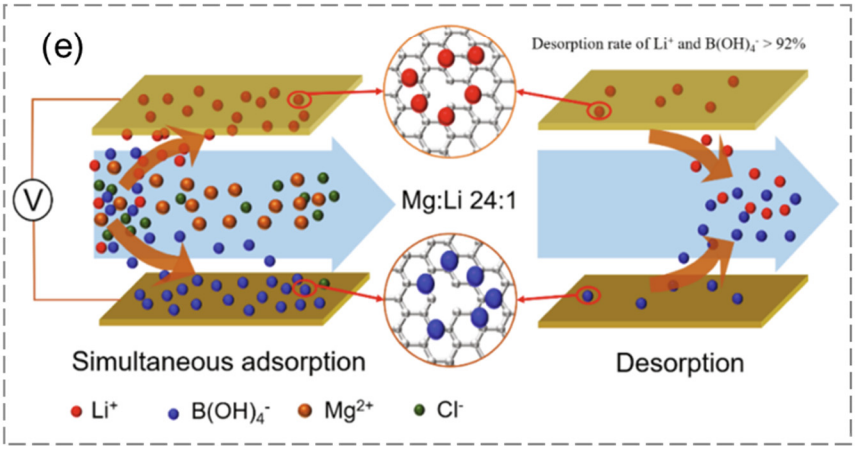


Figure 10. Various typical electrochemical lithium recovery reaction setups: (**a**) hybrid system with activated carbon; (**b**) hybrid system with polypyrrole; (**c**) Faraday system with rocking chair configuration; (**d**) faradic system with mixed-ion battery configuration [31,245–247]. (**e**) Schematic diagram of the electrochemical simultaneous adsorption and desorption process. Adapted with permission from Ref. [244]. 2021, Jin W.

4.2.2. Biological Nutrient Removal

The overuse of chemical fertilizers and the discharge of municipal and industrial effluents have resulted in the accumulation of nutrients in natural water, which has in turn led to environmental problems and serious damage to aquatic ecosystems. The content of nitrogen and phosphorus is an important indicator of water eutrophication. Traditional nutrient removal techniques include chemical precipitation, activated sludge, and adsorption. These processes often generate additional waste and cannot recover valuable nutrients, resulting in lower overall economic value [248–250]. Since most of the nutrients exist in water are in their ionic state, the CDI system can be used to selectively remove and recover the nutrients dissolved in the water, which has gradually attracted the attention of researchers [251–253].

Soluble nitrogen sources mainly exist in water in the form of NO_3^-/NO_2^- and NH_4^+. Researchers used FCDI technology to achieve efficient recovery of cationic NH_4^+ in low-concentration urban wastewater [83]. The effective ammonia nitrogen concentration can be increased by 20 times under the optimized operation condition, and the concentration of the brine stream can be as high as 322 mg·L^{-1}. The selective separation of cations by CEM is a key factor affecting the performance of FCDI system for ammonia nitrogen recovery. Fang et al. developed a novel stacked FCDI system using a monovalent cation selective exchange membrane (M-CEM) with K_2SO_4 as an additive for ammonia recovery [254]. The purity of the recovered product was increased from 50% to 80%, and the ammonia recovery rate was twice that of standard CEM (S-CEM). Kim et al. used two copper ferricyanide (CuHCF) electrodes with a large cubic crystal structure to construct a symmetric cell desalination system, and it exhibited 4.2 times higher selectivity for NH_4^+ than Na^+ [255]. Since the cell voltage is lower than 0.3 V, the system can achieve high-efficiency ammonia nitrogen recovery with low energy consumption (1.5 kWh·kg N^{-1}). The research results showed that CDI systems are a promising alternative technology for ammonia recovery, especially suitable for the enrichment and concentration of low-ammonia-containing influents. CDI also showed a good treatment effect in the removal of anionic NO_3^-/NO_2^-. In aqueous solutions where multiple ions coexist, achieving high-efficiency ion-selective separation is the core requirement of technological development. The study of CDI ion separation system by Lee et al. showed that the introduction of selective ion exchange resin can effectively enhance the affinity of CDI electrode for NO_3^- [256]. A novel resin rich in amino groups, BHP55, was coated on the surface of carbon electrodes to provide anion exchange function and higher selectivity for NO_3^- [257]. In addition, the flowing carbon

electrode can be used in CDI devices to recover ammonia resources from low-concentration wastewater. The dissolved ammonia salt $(NH_4)_2SO_2$ is first separated by the FCDI device under an electric field, and then gaseous ammonia is recovered in an acidic solution [258]. Although CDI exhibits a stronger effect for high-valence ions, studies have shown that, among monovalent anions (NO_3^-, Cl^-, F^-, Br^-) and cations (Na^+, K^+, NH_4^+), carbon electrodes are the most efficient for capturing NO_3^- and NH_4^+. The preference is due to the smaller hydration ratio (ratio of hydration radius to ionic radius) of NO_3^- and NH_4^+, which results in unique technical advantages of the CDI system in the application of nitrogen source recovery [259,260].

Phosphorus is another important nutrient element in water, which mainly exists in the form of phosphate. Eutrophication occurs when phosphate concentrations in natural water bodies exceed 0.1 $mg \cdot L^{-1}$ [261]. Recent studies have shown that FCDI can be applied for the removal and recovery of phosphorus from wastewater. When treating the phosphate feed stream with an initial concentration of 10 $mg \cdot L^{-1}$, the removal rate was as high as 97% under the voltage of 0–1.2 V [262]. As an important functional component of the FCDI phosphorus recovery system, the adsorption capacity of flow electrode particles for phosphate ions and the feasibility of recovery operations have become the research focus. David's group prepared a magnetic (Fe_3O_4) activated carbon particle and used it as an electrode for FCDI [263]. The magnetic carbon electrode could achieve selective adsorption of phosphate ions through a ligand exchange mechanism. In addition to electrode materials, the research group also conducted further product research on the phosphorus concentrate recovered from the FCDI system [264]. The FCDI system was coupled with the fluidized bed crystallization (FBC) system, such that the phosphorus concentrate was fixed in the crystallization column in the form of rhombohedron. FCDI was able to remove and concentrate 63% of the phosphorus, while the FBC system could fix 80% of the phosphorus as triangular or quadrilateral pellets under the optimized operating conditions. The research provides a worthy reference for the efficient recovery and productization of phosphorus from phosphorus-rich wastewater.

Since the actual phosphorus-containing wastewater usually contains many types of interfering ions, eliminating the interference of coexisting anions and realizing high-selective phosphorus recovery are essential for practical application. Xu et al. constructed a novel FCDI system with an integrated liquid membrane chamber and a pair of AEMs, which could selectively extract phosphorus and nitrogen from fresh human urine [265]. Negatively charged phosphorus ions (such as HPO_4^{2-} and $H_2PO_4^-$) can be captured by acidic extractants (such as HCl, HNO_3, and H_2SO_4) and converted into uncharged H_3PO_4, while other interfering ions such as Cl^- and SO_4^{2-} are excreted. Utilizing the competitive migration and protonation of ions, the system realized the highly selective recovery of phosphoric acid and nutrient salts. This research has reference significance for the application of FCDI in the field of nutrient salt recovery.

In general, some progress has been achieved within the research of CDI systems for biological nutrient recovery. Several recent studies have proven that CDI has a removal effect on ammonia and phosphate in water. Although vital analysis progress has been made, the study in this field remains in its initial stage, and more in-depth research is required to boost the selectivity and overall removal capability of CDI for nutrient salts [256]. Furthermore, the optimization of separation performance (i.e., ion selectivity, salt removal rate, and electrode adsorption capacity), system design (i.e., electrode, IEM, and cell configuration), and long-term stability (i.e., electrode–electrolyte separation, membrane fouling, and electrode capacity fading) is an issue that researchers need to further address in future studies. In addition, appropriate modeling techniques should be developed to predict the diffusion of nutrient ions in electric fields. The application of CDI for nutrient removal can be significantly improved by developing novel electrodes embedded, chelated, and redox-active materials.

4.3. Coupling System and Application

Although the low operating voltage of the CDI system enables its high energy efficiency, it also limits its ability to treat nonionic pollutants in practical applications. For complex water quality with various components, CDI can be coupled with other technologies to make up for each other's technical defects, so as to achieve the effect of surpassing the two technologies alone. Combining the inherent defects of the CDI system with the advantages of other existing technologies, several typical CDI coupling systems have been developed. The coupled CDI systems such as membrane separation [266], photocatalysis [267], and bioelectrochemistry [268] have synergistic effects between the two technologies. The performance in ion selective separation, wastewater treatment, energy recovery, etc. has been greatly improved.

RO is a pressure-driven membrane separation technology. By applying a pressure higher than the osmotic pressure to the solution on one side of the membrane, the solvent will reverse osmose against the direction of natural osmosis. The RO process needs to remove a larger proportion of water molecules from wastewater containing a small number of pollutants; although its ion removal rate is high and the effluent quality is good, it has disadvantages such as high energy consumption, low water recovery rate, and vulnerability to membrane pollution [269,270]. The use of the CDI system to further recover the brine after RO treatment can accurately combine the technical advantages of the two and achieve more efficient ion separation. Tao et al. developed an RO–CDI stage system (Figure 11a) [266]. When the feed stream was industrial brine without organic carbon (TOC), the fresh water was directly recovered by the RO module as product water, and the concentrated stream was further processed by the CDI module to obtain secondary recovery. However, when the TOC content in the feed stream was high (>20 mg·L^{-1}), the removal rate of TOC by the RO-CDI stage system was low, which led to membrane fouling of the IEMs and a decrease in the overall performance in the CDI system [271]. Therefore, the RO–CDI stage system is only suitable for the recovery of water from industrial and domestic wastewater. To overcome this limitation, a biologically activated carbon (BAC) pretreatment unit can be added between the RO-enriched brine and CDI. The researchers suggested setting up pretreatment technologies such as chemical precipitation and filtration before the CDI module, and developing organic removal methods, fouling control and cleaning methods, etc., so as to realize the continuous operation of the CDI coupling system.

Recent investigations on RO–CDI have shown its convincing and robust applicability for ultrapure water (UPW) production along with freshwater production. Minhas et al. [272] integrated RO and CDI technology for energy-efficient production of UPW and potable water from seawater. Under optimum feed conditions, the performance of the RO–CDI system was improved by operating a CDI module under the constant-current condition, allowing the production of a high quality and quantity of UPW. The reason for the raised UPW quantity is constant electronic flux bombarding the module, which results in continuous ions removal from saline water until the desired voltage is attained [47]. Chung et al. used FCDI technology to replace brackish water reverse osmosis (BWRO) system in the two-pass RO system, and investigated the feasibility of integration FCDI with RO [273]. In short, the study showed that, through the great removal efficiency of CDI technology, it can be used in UPW and freshwater production without remineralization. However, the energy efficiency of CDI technology compared with BWRO remains to be verified.

Photocatalysis is an advanced technology that directly utilizes solar energy to efficiently degrade organic pollutants in water. Since the system does not require additional energy, the development of photocatalysis has received extensive attention. However, the main target pollutants of photocatalysis are organic substances, and the process usually can only convert the forms of pollutants instead of completely removing the degradation products from water [274,275]. In contrast, CDI technology is mainly aimed at ionic impurities in water, which can completely remove charged pollutants from water, but cannot degrade the toxicity of organic pollutants. Therefore, coupling the two technologies can effectively overcome the restriction of every difference, while degrading and removing organic/inorganic

pollutants in water. Ye et al. coupled CDI with photocatalytic technology for simultaneous removal of organic pollutants and inorganic salts from wastewater (Figure 11b) [267]. A ternary film composed of g-C_3N_4 nanoparticles, self-assembled carbon nanotubes, and PVF foam was prepared. The assembled coupled system had a stable removal effect on both inorganic pollutants (55–81% and 32–65% for Na_2SO_4 and NaCl, respectively) and organic pollutants (100% for methylene blue dye).

A microbial fuel cell (MFC) is a complicated and advanced bioelectrochemical system, which uses electrons generated by electrogenic microorganisms to catalyze biochemical reactions during wastewater treatment to generate electricity [276]. Due to the low output voltage of MFC (0.5–0.8 V), the generated energy is difficult to be utilized directly [277]. Recent research has shown that MFCs can be used as energy supply systems to directly power other technologies that require low voltage. As a typical electrochemical system operating at low voltage, CDI is especially suitable for coupling with MFC. The electrical energy generated by MFC can supply energy for the CDI system, and the coupled system can effectively overcome the shortcomings of low degradation of organic in the CDI system [267]. The earliest reported MFC–CDI coupling system is the microbial desalination pond (MDC), where the electrolytic cell is divided into three compartments by a pair of IEMs. However, the technical drawbacks of MDC are its pH imbalance, low desalination efficiency, and easy accumulation of chloride ions in the anode compartment [276].

In response to the above problems, Forrestal et al. developed a microbial capacitive desalination cell (MCDC) for simultaneous production of energy from desalination [278]. The MCDC consisted of two CEMs, a current collector fabricated from nickel or copper mesh, and an activated carbon cloth for microorganism biofilm formation and ion adsorption, as shown in Figure 11c [279]. The desalination efficiency of MCDC was 7–25 times higher than that of CDI due to the potential generated in situ by microorganisms, and the salt removal rate was as high as about 69.4%. The study compared the MCDC and MDC systems. The pH of the MCDC cathode compartment was stable at 8.5, while the pH of the MDC increased from 7 to 11.4. In the desalination chamber, the pollutant removal rate of MCDC was higher than that of MDC (eighteen times TDS, five times COD). Although MFC–CDI coupling technology has significant advantages in ion removal, pollutant degradation, and electrical energy recovery, it is still limited to laboratory-scale studies [42]. Scale-up results in the high internal resistance of the MFC, which reduces the overall voltage output. To reduce the inner resistance of the MFC, miniature cells may be chosen, where the proximity between electrodes is reduced. Additionally, massive capacitors and reversible batteries can be used to store energy for future applications. To further advance the practical application of MFC–CDI coupling technology, parameters such as electrode material, reactor design, microbial community, and biofilm should be further optimized.

Benefiting from the synergy between different technologies, various CDI coupling systems effectively overcome the limitations of traditional CDI. It should be noted that, although some progress has been made in the research of coupled systems, there are still deficiencies in the practical application process, and most of them are limited to the laboratory scale. In the process of technical application, the actual water composition is complex, and there are certain fluctuations, which are very likely to affect the treatment effect of the coupled system. Therefore, further in-depth research and development of the CDI coupling system is required, which principally specializes in changes of the actual effluent, with special emphasis on the optimization of operating parameters and improvement of system performance and stability. In general, synchronously coupling CDI technology with other technologies to address each other's limitations is anticipated to utterly solve the issues in industrial water treatment systems.

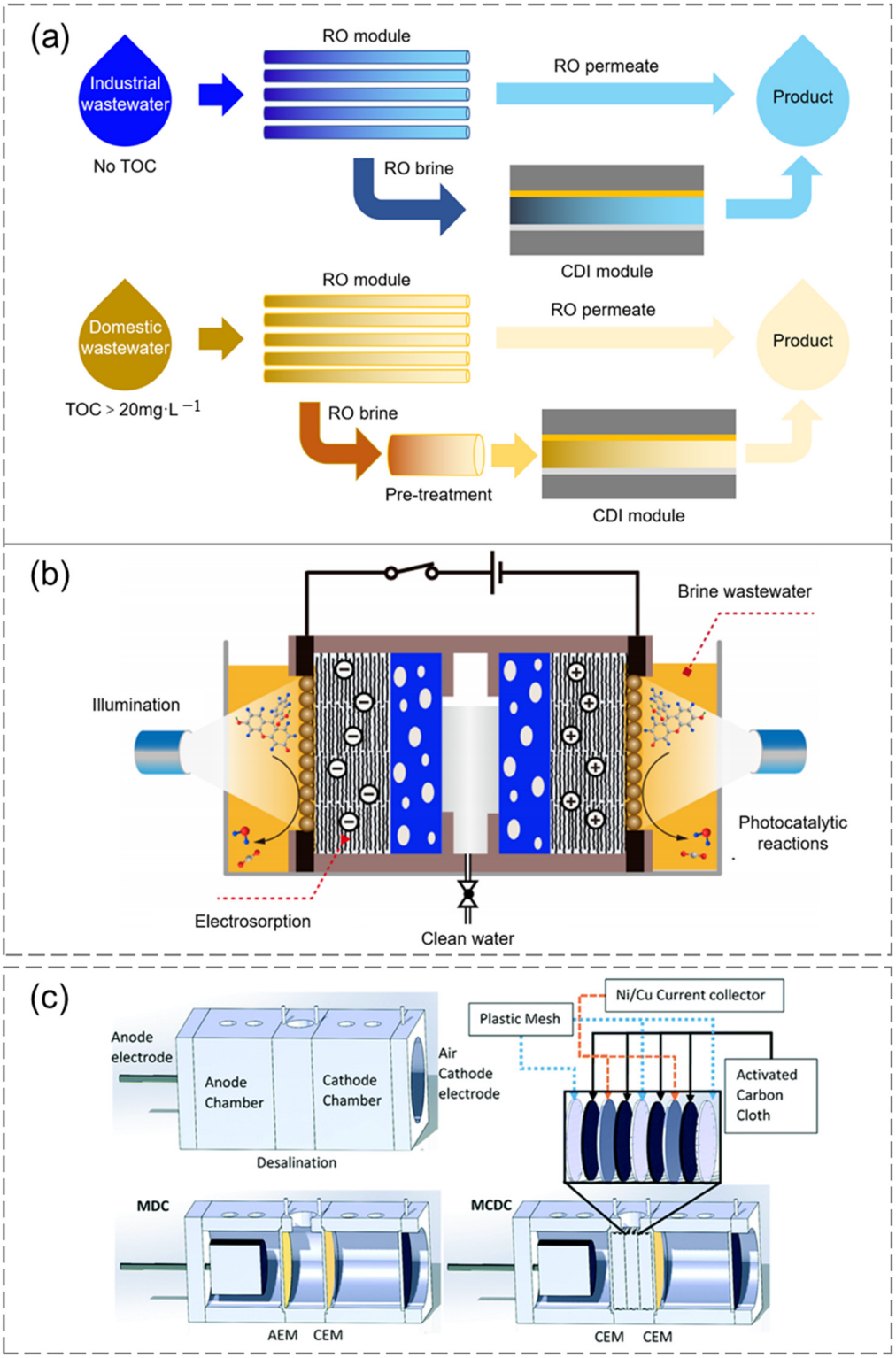


Figure 11. (**a**) Brackish water RO–CDI stage system without TOC concentration and schematic illustration of domestic wastewater RO–CDI hybrid system with TOC >20 mg·L^{-1}. Adapted with permission from Ref. [277]. 2019, Yamashita T; (**b**) integration of photocatalysis and CDI degradation of organic pollutants. Adapted with permission from Ref. [262]. 2020, Zhang J; (**c**) configuration of MDC (left) and MCDC (right). Adapted with permission from Ref. [276]. 2019, Zhang Y.

5. Conclusions and Outlook

CDI is an attractive electrically driven desalination technology with significant advantages over the existing desalination technologies; (i) ion removal at low voltage with mild operating conditions; (ii) the desalination process targets small amounts of ions in solution rather than large amounts of water, which leads to the higher overall energy efficiency; (iii) the potential application fields are broad. In this review, we comprehensively summarized the research progress of this advanced technology, with a specific focus on CDI desalination performance optimization strategies, system technoeconomic analysis, and existing and emerging application areas. Although CDI and its derived systems have made great progress in research in recent years, the development of this technology is still in its infancy, and there is still a large room for improvement. In order to further promote the practical application and transformation of CDI in various fields, we outline the current research challenges in this field and proposed directions for future research development.

First, the selective removal ability of CDI for specific target ions should be further improved. Although researchers have made significant progress in the development of CDI electrodes, the current performance evaluations of CDI electrodes are mostly limited to their salt removal efficiency, ion storage capacity, and long-term cycling stability, while few studies have been conducted on their selectivity. In the application of traditional CDI systems for desalination, the co-ion repulsion produces energy consumption. MCDI realizes the selective diffusion of ions in the system through the introduction of IEM, but problems such as IEM inherent resistance and interface contact resistance also cause unnecessary energy loss. Therefore, the development of electrodes with specific ion capture ability can effectively improve the energy efficiency of CDI desalination systems. In addition, the applications of specific ion selective removal and target ion recovery call for IEMs or electrodes with high ion selectivity, which is significant to further broaden the CDI application range. By constructing CDI systems with ion-selective capabilities, it is possible to preferentially eliminate highly toxic pollutants (such as heavy metals) in water/wastewater, or efficiently recover high-value resources (such as ammonia, phosphate, lithium, and other metals) from seawater or mining wastewater. Hence, ion-selective materials (including electrode materials and ion-exchange membranes) should be further investigated in the future.

Second, research on the energy efficiency of CDI desalination systems should be further focused. Since the ion removal mechanism is crucial for the energy efficiency of CDI systems, this review provided an overview of the adsorption mechanisms of CDI systems based on the GCS model and the modified Donnan model, as well as the ion intercalation or redox reaction mechanism based on the Faraday electrode. Since the energy efficiency of the CDI system is closely related to the concentration of the feed stream and the water quality requirements of the effluent, researchers have carried out systematic research on the control of applied current, battery voltage, feed stream concentration, pH value, etc. Further large-scale and long-term studies are required to obtain the feasibility of using CDI technology in practical applications. In addition, research on energy recovery is also beneficial to improve the competitiveness of the CDI system. It has been demonstrated that CDI systems can store energy during the ions adsorption process, as well as partly perform energy recovery during the regeneration process. However, the related research is only limited to the theoretical stage of laboratory scale, and it is necessary to further explore energy recovery systems to achieve improved energy efficiency desalination. Further research should also be focus on evaluation of economic cost of CDI technology.

Third, the application of CDI technology in different fields should be further explored. Early research on CDI technology mainly focused on the desalination of seawater or brackish water. In recent years, studies have turned to its application in the selective removal or recovery of specific ions. However, most CDI systems suffer from the limitation that they are only suitable for ionic substances. The research on CO_2 capture provided us with new ideas that the ionized gases in water can also be treated by CDI technology. In addition, this review summarized coupled systems of CDI combined with systems such

as membrane filtration, photocatalysis, and bioelectrochemistry. Due to the synergistic effect between the two processes, their limitations are avoided, so as to achieve the ideal water treatment effect. At present, the practical application of CDI is still in its initial stage. Future research should focus on the water quality diversity of the actual feed stream, as well as improving the performance and stability of the system under long-term operating conditions.

Funding: This research was funded by the National Natural Science Foundation of China (Nos. 52100075 and 52070035), the Jilin Province Scientific and the Technological Planning Project of China (No. 20220203009SF and 20200403001SF), and the Key Research and Development Project of Shandong Province (No. 2020CXGC011202).

Conflicts of Interest: The authors declare no conflict of interest.

References

1. Boretti, A.; Rosa, L. Reassessing the projections of the world water development report. *NPJ Clean Water* **2019**, *2*, 15. [CrossRef]
2. Oki, T.; Kanae, S. Global hydrological cycles and world water resources. *Science* **2006**, *313*, 1068–1072. [CrossRef]
3. Shannon, M.A.; Bohn, P.W.; Elimelech, M.; Georgiadis, J.G.; Marinas, B.J.; Mayes, A.M. Science and technology for water purification in the coming decades. *Nature* **2008**, *452*, 301–310. [CrossRef]
4. Van der Bruggen, B.; Vandecasteele, C. Distillation vs. membrane filtration: Overview of process evolutions in seawater desalination. *Desalination* **2002**, *143*, 207. [CrossRef]
5. Shaffer, D.L.; Arias Chavez, L.H.; Ben-Sasson, M.; Romero-Vargas Castrillón, S.; Yip, N.Y.; Elimelech, M. Desalination and reuse of high-salinity shale gas produced water: Drivers, technologies, and future directions. *Environ. Sci. Technol.* **2013**, *47*, 9569. [CrossRef]
6. Deshmukh, A.; Boo, C.; Karanikola, V.; Lin, S.W.; Straub, A.P.; Tong, T.; Warsinger, D.M.; Elimelech, M. Membrane distillation at the water-energy nexus: Limits, opportunities, and challenges. *Energy Environ. Sci.* **2018**, *11*, 1177. [CrossRef]
7. Elimelech, M.; Phillip, W.A. The future of seawater desalination: Energy, technology, and the environment. *Science* **2011**, *333*, 712–717. [CrossRef]
8. Fritzmann, C.; Löwenberg, J.; Wintgens, T.; Melin, T. State-of-the-art of reverse osmosis desalination. *Desalination* **2007**, *216*, 1–76. [CrossRef]
9. Strathmann, H. Electrodialysis, a mature technology with a multitude of new applications. *Desalination* **2010**, *264*, 268. [CrossRef]
10. Murphy, G.W.; Caudle, D.D. Mathematical theory of electrochemical demineralization in flowing systems. *Electrochim. Acta* **1967**, *12*, 1655–1664. [CrossRef]
11. Biesheuvel, P.M.; van Limpt, B.; Van der Wal, A. Dynamic adsorption/desorption process model for capacitive deionization. *J. Phys. Chem. C* **2009**, *113*, 5636. [CrossRef]
12. Bockris, J.O.M. The structure of water in the double layer. *Inorg. Chim. Acta* **1980**, *40*, X14. [CrossRef]
13. Zhao, R.; Biesheuvel, P.M.; Miedema, H.; Bruning, H.; van der Wal, A. Charge efficiency: A functional tool to probe the double-layer structure inside of porous electrodes and application in the modeling of capacitive deionization. *J. Phys. Chem. Lett.* **2010**, *1*, 205–210. [CrossRef]
14. Evans, S.; Hamilton, W.S. The mechanism of demineralization at carbon electrodes. *J. Electrochem. Soc.* **1966**, *113*, 1314. [CrossRef]
15. Biesheuvel, P.M.; Fu, Y.; Bazant, M.Z. Diffuse charge and Faradaic reactions in porous electrodes. *Phys. Rev. E* **2011**, *83*, 061507. [CrossRef]
16. Porada, S.; Borchardt, L.; Oschatz, M.; Bryjak, M.; Atchison, J.S.; Keesman, K.J.; Kaskel, S.; Biesheuvel, P.M.; Presser, V. Direct prediction of the desalination performance of porous carbon electrodes for capacitive deionization. *Energy Environ. Sci.* **2013**, *6*, 3700–3712. [CrossRef]
17. Porada, S.; Zhao, R.; van der Wal, A.; Presser, V.; Biesheuvel, P.M. Review on the science and technology of water desalination by capacitive deionization. *Prog. Mater. Sci.* **2013**, *58*, 1388–1442. [CrossRef]
18. Dykstra, J.E.; Porada, S.; van der Wal, A.; Biesheuvel, P.M. Energy consumption in capacitive deionization-constant current versus constant voltage operation. *Water Res.* **2018**, *143*, 367–375. [CrossRef]
19. Lee, J.B.; Park, K.K.; Eum, H.M.; Lee, C.W. Desalination of a thermal power plant wastewater by membrane capacitive deionization. *Desalination* **2006**, *196*, 125–134. [CrossRef]
20. Jeon, S.-I.; Park, H.-R.; Yeo, J.-G.; Yang, S.; Cho, C.H.; Han, M.H.; Kim, D.K. Desalination via a new membrane capacitive deionization process utilizing flow-electrodes. *Energy Environ. Sci.* **2013**, *6*, 1471–1475. [CrossRef]
21. Wang, L.; Wang, M.; Huang, Z.-H.; Cui, T.; Gui, X.; Kang, F.; Wang, K.; Wu, D. Capacitive deionization of NaCl solutions using carbon nanotube sponge electrodes. *J. Mater. Chem.* **2011**, *21*, 18295–18299. [CrossRef]
22. Li, Z.; Song, B.; Wu, Z.; Lin, Z.; Yao, Y.; Moon, K.-S.; Wong, C.P. 3D porous graphene with ultrahigh surface area for microscale capacitive deionization. *Nano Energy* **2015**, *11*, 711–718. [CrossRef]

23. Xu, X.T.; Allah, A.E.; Wang, C.; Tan, H.B.; Farghali, A.A.; Khedr, M.H.; Malgras, V.; Yang, T.; Yamauchi, Y. Capacitive deionization using nitrogen-doped mesostructured carbons for highly efficient brackish water desalination. *Chem. Eng. J.* **2019**, *362*, 887–896. [CrossRef]
24. Kumar, R.; Sen Gupta, S.; Katiyar, S.; Raman, V.K.; Varigala, S.K.; Pradeep, T.; Sharma, A. Carbon aerogels through organo-inorganic co-assembly and their application in water desalination by capacitive deionization. *Carbon* **2016**, *99*, 375–383. [CrossRef]
25. Beguin, F.; Presser, V.; Balducci, A.; Frackowiak, E. Carbons and electrolytes for advanced supercapacitors. *Adv. Mater.* **2014**, *26*, 2219–2251. [CrossRef]
26. Lee, J.; Kim, S.; Kim, C.; Yoon, J. Hybrid capacitive deionization to enhance the desalination performance of capacitive techniques. *Energy Environ. Sci.* **2014**, *7*, 3683–3689. [CrossRef]
27. Suss, M.E.; Presser, V. Water desalination with energy storage electrode materials. *Joule* **2018**, *2*, 10–15. [CrossRef]
28. Choi, S.; Chang, B.; Kim, S.; Lee, J.; Yoon, J.; Choi, J.W. Battery electrode materials with omnivalent cation storage for fast and charge-efficient ion removal of asymmetric capacitive deionization. *Adv. Funct. Mater.* **2018**, *28*, 1802665. [CrossRef]
29. Yoon, H.; Lee, J.; Kim, S.-R.; Kang, J.; Kim, S.; Kim, C.; Yoon, J. Capacitive deionization with Ca-alginate coated-carbon electrode for hardness control. *Desalination* **2016**, *392*, 46–53. [CrossRef]
30. Choi, J.; Dorji, P.; Shon, H.K.; Hong, S. Applications of capacitive deionization: Desalination, softening, selective removal, and energy efficiency. *Desalination* **2019**, *449*, 118–130. [CrossRef]
31. Lee, J.; Yu, S.-H.; Kim, C.; Sung, Y.-E.; Yoon, J. Highly selective lithium recovery from brine using a lambda-MnO_2-Ag battery. *Phys. Chem. Chem. Phys.* **2013**, *15*, 7690–7695. [CrossRef] [PubMed]
32. Siekierka, A.; Tomaszewska, B.; Bryjak, M. Lithium capturing from geothermal water by hybrid capacitive deionization. *Desalination* **2018**, *436*, 8–14. [CrossRef]
33. Pasta, M.; Battistel, A.; La Mantia, F. Batteries for lithium recovery from brines. *Energy Environ. Sci.* **2012**, *5*, 9487–9491. [CrossRef]
34. Trocoli, R.; Battistel, A.; La Mantia, F. Nickel hexacyanoferrate as suitable alternative to Ag for electrochemical lithium recovery. *ChemSusChem* **2015**, *8*, 2514–2519. [CrossRef]
35. Kim, S.; Kim, J.; Kim, S.; Lee, J.; Yoon, J. Electrochemical lithium recovery and organic pollutant removal from industrial wastewater of a battery recycling plant. *Environ. Sci. Water Res. Technol.* **2018**, *4*, 175–182. [CrossRef]
36. Kim, S.; Yoon, H.; Shin, D.; Lee, J.; Yoon, J. Electrochemical selective ion separation in capacitive deionization with sodium manganese oxide. *J. Colloid Interface Sci.* **2017**, *506*, 644–648. [CrossRef] [PubMed]
37. Yoon, H.; Lee, J.; Kim, S.; Yoon, J. Electrochemical sodium ion impurity removal system for producing high purity KCl. *Hydrometallurgy* **2018**, *175*, 354–358. [CrossRef]
38. Farmer, J.C.; Fix, D.V.; Mack, G.V.; Pekala, R.W.; Poco, J.F. Capacitive deionization of NH_4ClO_4 solutions with carbon aerogel electrodes. *J. Appl. Electrochem.* **1996**, *26*, 1007–1018. [CrossRef]
39. Farmer, J.C.; Fix, D.V.; Mack, G.V.; Pekala, R.W.; Poco, J.F. Capacitive deionization of NaCl and $NaNO_3$ solutions with carbon aerogel electrodes. *J. Electrochem. Soc.* **1996**, *143*, 159–169. [CrossRef]
40. Legrand, L.; Shu, Q.; Tedesco, M.; Dykstra, J.E.; Hamelers, H.V.M. Role of ion exchange membranes and capacitive electrodes in membrane capacitive deionization (MCDI) for CO_2 capture. *J. Colloid Interface Sci.* **2020**, *564*, 478–490. [CrossRef]
41. Legrand, L.; Schaetzle, O.; de Kler, R.C.F.; Hamelers, H.V.M. Solvent-free CO_2 capture using membrane capacitive deionization. *Environ. Sci. Technol.* **2018**, *52*, 9478–9485. [CrossRef] [PubMed]
42. Dahiya, S.; Singh, A.; Mishra, B.K. Capacitive deionized hybrid systems for wastewater treatment and desalination: A review on synergistic effects, mechanisms and challenges. *Chem. Eng. J.* **2021**, *417*, 128129. [CrossRef]
43. AlMarzooqi, F.A.; Al Ghaferi, A.A.; Saadat, I.; Hilal, N. Application of capacitive deionization in water desalination: A review. *Desalination* **2014**, *342*, 3–15. [CrossRef]
44. Zhao, X.; Yang, H.; Wang, Y.; Sha, Z. Review on the electrochemical extraction of lithium from seawater/brine. *J. Electroanal. Chem.* **2019**, *850*, 113389. [CrossRef]
45. Długołęcki, P.; van der Wal, A. Energy recovery in membrane capacitive deionization. *Environ. Sci. Technol.* **2013**, *47*, 4904–4910. [CrossRef] [PubMed]
46. Kang, J.; Kim, T.; Shin, H.; Lee, J.; Ha, J.-I.; Yoon, J. Direct energy recovery system for membrane capacitive deionization. *Desalination* **2016**, *398*, 144–150. [CrossRef]
47. Zhao, R.; Biesheuvel, P.M.; van der Wal, A. Energy consumption and constant current operation in membrane capacitive deionization. *Energy Environ. Sci.* **2012**, *5*, 9520–9527. [CrossRef]
48. Porada, S.; Bryjak, M.; van der Wal, A.; Biesheuvel, P.M. Effect of electrode thickness variation on operation of capacitive deionization. *Electrochim. Acta* **2012**, *75*, 148–156. [CrossRef]
49. Zhao, R.; van Soestbergen, M.; Rijnaarts, H.H.M.; van der Wal, A.; Bazant, M.Z.; Biesheuvel, P.M. Time-dependent ion selectivity in capacitive charging of porous electrodes. *J. Colloid Interface Sci.* **2012**, *384*, 38–44. [CrossRef]
50. Kamran, K.; van Soestbergen, M.; Pel, L. Electrokinetic salt removal from porous building materials using ion exchange membranes. *Transp. Porous Med.* **2013**, *96*, 221–235. [CrossRef]
51. Biesheuvel, P.M.; Fu, Y.; Bazant, M.Z. Electrochemistry and capacitive charging of porous electrodes in asymmetric multicomponent electrolytes. *Russ. J. Electrochem.* **2012**, *48*, 580–592. [CrossRef]
52. Kastening, B.; Heins, M. Properties of electrolytes in the micropores of activated carbon. *Electrochim. Acta* **2005**, *50*, 2487–2498. [CrossRef]

53. Arafat, H.A.; Franz, M.; Pinto, N.G. Effect of salt on the mechanism of adsorption of aromatics on activated carbon. *Langmuir* **1999**, *15*, 5997–6003. [CrossRef]
54. Liu, E.; Lee, L.Y.; Ong, S.L.; Ng, H.Y. Treatment of industrial brine using capacitive deionization (CDI) towards zero liquid discharge-challenges and optimization. *Water Res.* **2020**, *183*, 116059. [CrossRef]
55. Xu, X.; Wang, M.; Liu, Y.; Lu, T.; Pan, L. Ultrahigh desalinization performance of asymmetric flow-electrode capacitive deionization device with an improved operation voltage of 1.8 V. *ACS Sustain. Chem. Eng.* **2017**, *5*, 189–195. [CrossRef]
56. Andres, G.L.; Yoshihara, Y. A capacitive deionization system with high energy recovery and effective re-use. *Energy* **2016**, *103*, 605–617. [CrossRef]
57. Hou, C.H.; Liu, N.L.; Hsu, H.L.; Den, W. Development of multi-walled carbon nanotube/poly(vinyl alcohol) composite as electrode for capacitive deionization. *Sep. Purif. Technol.* **2014**, *130*, 7–14. [CrossRef]
58. Srimuk, P.; Kaasik, F.; Kruener, B.; Tolosa, A.; Fleischmann, S.; Jaeckel, N.; Tekeli, M.C.; Aslan, M.; Suss, M.E.; Presser, V. MXene as a novel intercalation-type pseudocapacitive cathode and anode for capacitive deionization. *J. Mater. Chem. A* **2016**, *4*, 18265–18271. [CrossRef]
59. Lee, J.; Srimuk, P.; Zwingelstein, R.; Zornitta, R.L.; Choi, J.; Kim, C.; Presser, V. Sodium ion removal by hydrated vanadyl phosphate for electrochemical water desalination supplementary information (ESI) available. *J. Mater. Chem. A* **2019**, *7*, 4175–4184. [CrossRef]
60. Tan, C.; He, C.; Fletcher, J.; Waite, T.D. Energy recovery in pilot scale membrane CDI treatment of brackish waters. *Water Res.* **2020**, *168*, 115146. [CrossRef]
61. Zhan, F.; Wang, Z.; Wu, T.; Dong, Q.; Zhao, C.; Wang, G.; Qiu, J. High performance concentration capacitors with graphene hydrogel electrodes for harvesting salinity gradient energy. *J. Mater. Chem. A* **2018**, *6*, 4981–4987. [CrossRef]
62. Tang, W.; He, D.; Zhang, C.; Kovalsky, P.; Waite, T.D. Comparison of Faradaic reactions in capacitive deionization (CDI) and membrane capacitive deionization (MCDI) water treatment processes. *Water Res.* **2017**, *120*, 229–237. [CrossRef] [PubMed]
63. Lee, J.-H.; Bae, W.-S.; Choi, J.-H. Electrode reactions and adsorption/desorption performance related to the applied potential in a capacitive deionization process. *Desalination* **2010**, *258*, 159–163. [CrossRef]
64. Biesheuvel, P.M.; Porada, S.; Levi, M.; Bazant, M.Z. Attractive forces in microporous carbon electrodes for capacitive deionization. *J. Solid State Electrochem.* **2014**, *18*, 1365–1376. [CrossRef]
65. Wang, C.M.; Song, H.O.; Zhang, Q.X.; Wang, B.J.; Li, A.M. Parameter optimization based on capacitive deionization for highly efficient desalination of domestic wastewater biotreated effluent and the fouled electrode regeneration. *Desalination* **2015**, *365*, 407–415. [CrossRef]
66. Mossad, M.; Zou, L. Study of fouling and scaling in capacitive deionization by using dissolved organic and inorganic salts. *J. Hazard. Mater.* **2013**, *244*, 387–393. [CrossRef]
67. Wang, Z.Q.; Wang, Y.; Ma, D.Y.; Xu, S.C.; Wang, J.X. Investigations on the fouling characteristics of ion-doped polypyrrole/carbon nanotube composite electrodes in capacitive deionization by using half cycle running mode. *Sep. Purif. Technol.* **2018**, *192*, 15–20. [CrossRef]
68. Luo, J.; Tian, D.; Ding, Z.; Lu, T.; Xu, X.; Pan, L. Enhanced cycling stability of capacitive deionization via effectively inhibiting H_2O_2 formation: The role of nitrogen dopants. *J. Electroanal. Chem.* **2019**, *855*, 113488. [CrossRef]
69. Biesheuvel, P.M.; Zhao, R.; Porada, S.; van der Wal, A. Theory of membrane capacitive deionization including the effect of the electrode pore space. *J. Colloid Interface Sci.* **2011**, *360*, 239–248. [CrossRef]
70. Li, H.; Zou, L. Ion-exchange membrane capacitive deionization: A new strategy for brackish water desalination. *Desalination* **2011**, *275*, 62–66. [CrossRef]
71. Laxman, K.; Myint, M.; Abri, M.A.; Sathe, P.; Dobretsov, S.; Dutta, J. Desalination and disinfection of inland brackish ground water in a capacitive deionization cell using nanoporous activated carbon cloth electrodes. *Desalination* **2015**, *362*, 126–132. [CrossRef]
72. Zhang, C.Y.; He, D.; Ma, J.X.; Tang, W.W.; Waite, T.D. Faradaic reactions in capacitive deionization (CDI)-problems and possibilities: A review. *Water Res.* **2018**, *128*, 314–330. [CrossRef] [PubMed]
73. Li, P.; Gui, Y.; Blackwood, D.J. Development of a nanostructured alpha-MnO_2/carbon paper composite for removal of Ni^{2+}/Mn^{2+} ions by electrosorption. *ACS Appl. Mater. Interfaces* **2018**, *10*, 19615–19625. [CrossRef] [PubMed]
74. Alaei Shahmirzadi, M.A.; Hosseini, S.S.; Luo, J.; Ortiz, I. Significance, evolution and recent advances in adsorption technology, materials and processes for desalination, water softening and salt removal. *J. Environ. Manag.* **2018**, *215*, 324–344. [CrossRef]
75. Yang, S.; Choi, J.; Yeo, J.-G.; Jeon, S.-I.; Park, H.-R.; Kim, D.K. Flow-electrode capacitive deionization using an aqueous electrolyte with a high salt concentration. *Environ. Sci. Technol.* **2016**, *50*, 5892–5899. [CrossRef] [PubMed]
76. Suss, M.E.; Porada, S.; Sun, X.; Biesheuvel, P.M.; Yoon, J.; Presser, V. Water desalination via capacitive deionization: What is it and what can we expect from it? *Energy Environ. Sci.* **2015**, *8*, 2296–2319. [CrossRef]
77. Biesheuvel, P.M.; van der Wal, A. Membrane capacitive deionization. *J. Membr. Sci.* **2010**, *346*, 256–262. [CrossRef]
78. Park, H.R.; Choi, J.; Yang, S.; Kwak, S.J.; Jeon, S.I.; Han, M.H.; Kim, D.K. Surface-modified spherical activated carbon for high carbon loading and its desalting performance in flow-electrode capacitive deionization. *RSC Adv.* **2016**, *6*, 69720–69727. [CrossRef]
79. Liang, P.; Sun, X.; Bian, Y.; Zhang, H.; Yang, X.; Jiang, Y.; Liu, P.; Huang, X. Optimized desalination performance of high voltage flow-electrode capacitive deionization by adding carbon black in flow-electrode. *Desalination* **2017**, *420*, 63–69. [CrossRef]
80. Rommerskirchen, A.; Gendel, Y.; Wessling, M. Single module flow-electrode capacitive deionization for continuous water desalination. *Electrochem. Commun.* **2015**, *60*, 34–37. [CrossRef]

81. Gendel, Y.; Rommerskirchen, A.K.E.; David, O.; Wessling, M. Batch mode and continuous desalination of water using flowing carbon deionization (FCDI) technology. *Electrochem. Commun.* **2014**, *46*, 152–156. [CrossRef]
82. Rommerskirchen, A.; Linnartz, C.J.; Muller, D.; Willenberg, L.K.; Wessling, M. Energy recovery and process design in continuous flow electrode capacitive deionization processes. *ACS Sustain. Chem. Eng.* **2018**, *6*, 13007–13015. [CrossRef]
83. Fang, K.; Gong, H.; He, W.; Peng, F.; He, C.; Wang, K. Recovering ammonia from municipal wastewater by flow-electrode capacitive deionization. *Chem. Eng. J.* **2018**, *348*, 301–309. [CrossRef]
84. He, C.; Ma, J.; Zhang, C.; Song, J.; Waite, T.D. Short-circuited closed-cycle operation of flow-electrode CDI for brackish water softening. *Environ. Sci. Technol.* **2018**, *52*, 9350–9360. [CrossRef] [PubMed]
85. Ma, J.X.; He, C.; He, D.; Zhang, C.Y.; Waite, T.D. Analysis of capacitive and electrodialytic contributions to water desalination by flow-electrode CDI. *Water Res.* **2018**, *144*, 296–303. [CrossRef]
86. Yang, S.C.; Kim, H.; Jeon, S.I.; Choi, J.; Yeo, J.G.; Park, H.R.; Jin, J.; Kim, D.K. Analysis of the desalting performance of flow-electrode capacitive deionization under short-circuited closed cycle operation. *Desalination* **2017**, *424*, 110–121. [CrossRef]
87. Yang, S.C.; Jeon, S.-i.; Kim, H.; Choi, J.; Yeo, J.-g. Stack design and operation for scaling up the capacity of flow-electrode capacitive deionization technology. *ACS Sustain. Chem. Eng.* **2016**, *4*, 4174–4180. [CrossRef]
88. Lee, K.S.; Cho, Y.; Choo, K.Y.; Yang, S.; Han, M.H.; Kim, D.K. Membrane-spacer assembly for flow-electrode capacitive deionization. *Appl. Surf. Sci.* **2018**, *433*, 437–442. [CrossRef]
89. Yang, S.C.; Park, H.R.; Yoo, J.; Kim, H.; Choi, J.; Han, M.H.; Kim, D.K. Plate-shaped graphite for improved performance of flow-electrode capacitive deionization. *J. Electrochem. Soc.* **2017**, *164*, E480–E488. [CrossRef]
90. Pasta, M.; Wessells, C.D.; Cui, Y.; La Mantia, F. A desalination battery. *Nano Lett.* **2012**, *12*, 839–843. [CrossRef]
91. Chen, F.; Huang, Y.; Guo, L.; Sun, L.; Wang, Y.; Yang, H.Y. Dual-ions electrochemical deionization: A desalination generator. *Energy Environ. Sci.* **2017**, *10*, 2081–2089. [CrossRef]
92. Nam, D.H.; Choi, K.S. Bismuth as a New Chloride-storage electrode enabling the construction of a practical high capacity desalination battery. *J. Am. Chem. Soc.* **2017**, *139*, 11055–11063. [CrossRef] [PubMed]
93. Hand, S.; Cusick, R.D. Characterizing the impacts of deposition techniques on the performance of MnO_2 cathodes for sodium electrosorption in hybrid capacitive deionization. *Environ. Sci. Technol.* **2017**, *51*, 12027–12034. [CrossRef]
94. Wu, T.T.; Wang, G.; Wang, S.Y.; Zhan, F.; Fu, Y.; Qiao, H.Y.; Qiu, J.S. Highly stable hybrid capacitive deionization with a MnO_2 anode and a positively charged cathode. *Environ. Sci. Technol. Lett.* **2018**, *5*, 98–102. [CrossRef]
95. Yang, S.; Luo, M. In-situ embedding ZrO_2 nanoparticles in hierarchically porous carbon matrix as electrode materials for high desalination capacity of hybrid capacitive deionization. *Mater. Lett.* **2019**, *248*, 197–200. [CrossRef]
96. Zhao, C.; Wang, X.; Zhang, S.; Sun, N.; Zhou, H.; Wang, G.; Zhang, Y.; Zhang, H.; Zhao, H. Porous carbon nanosheets functionalized with Fe_3O_4 nanoparticles for capacitive removal of heavy metal ions from water. *Environ. Sci. Water Res. Technol.* **2020**, *6*, 331–340. [CrossRef]
97. Ma, X.; Chen, Y.A.; Zhou, K.F.; Wu, P.C.; Hou, C.H. Enhanced desalination performance via mixed capacitive-Faradaic ion storage using RuO_2-activated carbon composite electrodes. *Electrochim. Acta* **2019**, *295*, 769–777. [CrossRef]
98. Li, J.; Yan, D.; Hou, S.; Li, Y.; Lu, T.; Yao, Y.; Pan, L. Improved sodium-ion storage performance of $Ti_3C_2T_x$ MXenes by sulfur doping. *J. Mater. Chem. A* **2018**, *6*, 1234–1243. [CrossRef]
99. Srimuk, P.; Halim, J.; Lee, J.; Tao, Q.Z.; Rosen, J.; Presser, V. Two-dimensional molybdenum carbide (MXene) with divacancy ordering for brackish and seawater desalination via cation and anion intercalation. *ACS Sustain. Chem. Eng.* **2018**, *6*, 3739–3747. [CrossRef]
100. Torkamanzadeh, M.; Wang, L.; Zhang, Y.; Budak, Ö.; Srimuk, P.; Presser, V. MXene/Activated-carbon hybrid capacitive deionization for permselective ion removal at low and high salinity. *ACS Appl. Mater. Interfaces* **2020**, *12*, 26013–26025. [CrossRef]
101. Bao, W.; Liu, L.; Wang, C.; Choi, S.; Wang, D.; Wang, G. Facile synthesis of crumpled nitrogen-doped MXene nanosheets as a new sulfur host for lithium–sulfur batteries. *Adv. Energy Mater.* **2018**, *8*, 1702485. [CrossRef]
102. Srimuk, P.; Lee, J.; Fleischmann, S.; Choudhury, S.; Jackel, N.; Zeiger, M.; Kim, C.; Aslan, M.; Presser, V. Faradaic deionization of brackish and sea water via pseudocapacitive cation and anion intercalation into few-layered molybdenum disulfide. *J. Mater. Chem. A* **2017**, *5*, 15640–15649. [CrossRef]
103. Bao, W.Z.; Tang, X.; Guo, X.; Choi, S.; Wang, C.Y.; Gogotsi, Y.; Wang, G.X. Porous cryo-dried MXene for efficient capacitive deionization. *Joule* **2018**, *2*, 778–787. [CrossRef]
104. Wang, H.-G.; Li, W.; Liu, D.-P.; Feng, X.-L.; Wang, J.; Yang, X.-Y.; Zhang, X.-B.; Zhu, Y.; Zhang, Y. Flexible electrodes for sodium-ion batteries: Recent progress and perspectives. *Adv. Mater.* **2017**, *29*, 1703012. [CrossRef] [PubMed]
105. Kim, C.; Srimuk, P.; Lee, J.; Fleischmann, S.; Aslan, M.; Presser, V. Influence of pore structure and cell voltage of activated carbon cloth as a versatile electrode material for capacitive deionization. *Carbon* **2017**, *122*, 329–335. [CrossRef]
106. Bouhadana, Y.; Avraham, E.; Noked, M.; Ben-Tzion, M.; Soffer, A.; Aurbach, D. Capacitive deionization of NaCl solutions at non-steady-state conditions: Inversion functionality of the carbon electrodes. *J. Phys. Chem. C* **2011**, *115*, 16567–16573. [CrossRef]
107. Avraham, E.; Noked, M.; Soffer, A.; Aurbach, D. The feasibility of boron removal from water by capacitive deionization. *Electrochim. Acta* **2011**, *56*, 6312–6317. [CrossRef]
108. Guo, L.; Kong, D.; Pam, M.E.; Huang, S.; Ding, M.; Shang, Y.; Gu, C.; Huang, Y.; Yang, H.Y. The efficient Faradaic Li4Ti5O12@C electrode exceeds the membrane capacitive desalination performance. *J. Mater. Chem. A* **2019**, *7*, 8912–8921. [CrossRef]

109. Liu, P.; Yan, T.; Shi, L.; Park, H.S.; Chen, X.; Zhao, Z.; Zhang, D. Graphene-based materials for capacitive deionization. *J. Mater. Chem. A* **2017**, *5*, 13907–13943. [CrossRef]
110. Khan, Z.U.; Yan, T.; Han, J.; Shi, L.; Zhang, D. Capacitive deionization of saline water using graphene nanosphere decorated N-doped layered mesoporous carbon frameworks. *Environ. Sci. Nano* **2019**, *6*, 3442–3453. [CrossRef]
111. Duan, H.; Yan, T.; Chen, G.; Zhang, J.; Shi, L.; Zhang, D. A facile strategy for the fast construction of porous graphene frameworks and their enhanced electrosorption performance. *Chem. Commun.* **2017**, *53*, 7465–7468. [CrossRef] [PubMed]
112. Liu, P.; Yan, T.; Zhang, J.; Shi, L.; Zhang, D. Separation and recovery of heavy metal ions and salt ions from wastewater by 3D graphene-based asymmetric electrodes via capacitive deionization. *J. Mater. Chem. A* **2017**, *5*, 14748–14757. [CrossRef]
113. Li, C.; Zhang, X.; Wang, K.; Sun, X.; Liu, G.; Li, J.; Tian, H.; Li, J.; Ma, Y. Scalable self-propagating high-temperature synthesis of graphene for supercapacitors with superior power density and cyclic stability. *Adv. Mater.* **2017**, *29*, 1604690. [CrossRef] [PubMed]
114. Yan, T.; Liu, J.; Lei, H.; Shi, L.; An, Z.; Park, H.S.; Zhang, D. Capacitive deionization of saline water using sandwich-like nitrogen-doped graphene composites via a self-assembling strategy. *Environ. Sci. Nano* **2018**, *5*, 2722–2730. [CrossRef]
115. Khan, Z.U.; Yan, T.; Shi, L.; Zhang, D. Improved capacitive deionization by using 3D intercalated graphene sheet–sphere nanocomposite architectures. *Environ. Sci. Nano* **2018**, *5*, 980–991. [CrossRef]
116. Huang, Y.X.; Chen, F.M.; Guo, L.; Yang, H.Y. Ultrahigh performance of a novel electrochemical deionization system based on a $NaTi_2(PO_4)_3$/rGO nanocomposite. *J. Mater. Chem. A* **2017**, *5*, 18157–18165. [CrossRef]
117. Lee, B.; Park, N.; Kang, K.S.; Ryu, H.J.; Hong, S.H. Enhanced Capacitive deionization by dispersion of CNTs in activated carbon dlectrode. *ACS Sustain. Chem. Eng.* **2018**, *6*, 1572–1579. [CrossRef]
118. Xu, X.; Liu, Y.; Lu, T.; Sun, Z.; Chua, D.H.C.; Pan, L. Rational design and fabrication of graphene/carbon nanotubes hybrid sponge for high-performance capacitive deionization. *J. Mater. Chem. A* **2015**, *3*, 13418–13425. [CrossRef]
119. Moronshing, M.; Subramaniam, C. Scalable approach to highly efficient and rapid capacitive deionization with CNT-thread as electrodes. *ACS Appl. Mater. Interfaces* **2017**, *9*, 39907–39915. [CrossRef]
120. Vinod, S.; Tiwary, C.S.; Machado, L.D.; Ozden, S.; Vajtai, R.; Galvao, D.S.; Ajayan, P.M. Synthesis of ultralow density 3D graphene-CNT foams using a two-step method. *Nanoscale* **2016**, *8*, 15857–15863. [CrossRef]
121. Sriramulu, D.; Yang, H.Y. Free-standing flexible film as a binder-free electrode for an efficient hybrid deionization system. *Nanoscale* **2019**, *11*, 5896–5908. [CrossRef] [PubMed]
122. Li, H.; Gao, Y.; Pan, L.; Zhang, Y.; Chen, Y.; Sun, Z. Electrosorptive desalination by carbon nanotubes and nanofibres electrodes and ion-exchange membranes. *Water Res.* **2008**, *42*, 4923–4928. [CrossRef] [PubMed]
123. Xu, X.T.; Wang, M.; Liu, Y.; Lu, T.; Pan, L.K. Metal-organic framework-engaged formation of a hierarchical hybrid with carbon nanotube inserted porous carbon polyhedra for highly efficient capacitive deionization. *J. Mater. Chem. A* **2016**, *4*, 5467–5473. [CrossRef]
124. Nie, C.; Pan, L.; Liu, Y.; Li, H.; Chen, T.; Lu, T.; Sun, Z. Electrophoretic deposition of carbon nanotubes–polyacrylic acid composite film electrode for capacitive deionization. *Electrochim. Acta* **2012**, *66*, 106–109. [CrossRef]
125. Gao, T.; Zhou, F.; Ma, W.; Li, H. Metal-organic-framework derived carbon polyhedron and carbon nanotube hybrids as electrode for electrochemical supercapacitor and capacitive deionization. *Electrochim. Acta* **2018**, *263*, 85–93. [CrossRef]
126. Srimuk, P.; Lee, J.; Fleischmann, S.; Aslan, M.; Kim, C.; Presser, V. Potential-dependent, switchable ion selectivity in aqueous media using titanium disulfide. *Chemsuschem* **2018**, *11*, 2091–2100. [CrossRef]
127. Agartan, L.; Hantanasirisakul, K.; Buczek, S.; Akuzum, B.; Mahmoud, K.A.; Anasori, B.; Gogotsi, Y.; Kumbur, E.C. Influence of operating conditions on the desalination performance of a symmetric pre-conditioned $Ti_3C_2T_x$-MXene membrane capacitive deionization system. *Desalination* **2020**, *477*, 114267. [CrossRef]
128. Lee, J.; Kim, S.; Yoon, J. Rocking chair desalination battery based on prussian blue electrodes. *ACS Omega* **2017**, *2*, 1653–1659. [CrossRef]
129. Porada, S.; Shrivastava, A.; Bukowska, P.; Biesheuvel, P.M.; Smith, K.C. Nickel hexacyanoferrate electrodes for continuous cation intercalation desalination of brackish water. *Electrochim. Acta* **2017**, *255*, 369–378. [CrossRef]
130. Kim, T.; Gorski, C.A.; Logan, B.E. Low energy desalination using battery electrode deionization. *Environ. Sci. Technol. Lett.* **2017**, *4*, 444–449. [CrossRef]
131. Vafakhah, S.; Beiramzadeh, Z.; Saeedikhani, M.; Yang, H.Y. A review on free-standing electrodes for energy-effective desalination: Recent advances and perspectives in capacitive deionization. *Desalination* **2020**, *493*, 114662. [CrossRef]
132. Li, X.; Huang, Z.; Shuck, C.E.; Liang, G.; Gogotsi, Y.; Zhi, C. MXene chemistry, electrochemistry and energy storage applications. *Nat. Rev. Chem.* **2022**, *6*, 389–404. [CrossRef]
133. Kim, S.; Lee, J.; Kim, C.; Yoon, J. Na2FeP2O7 as a novel material for hybrid capacitive deionization. *Electrochim. Acta* **2016**, *203*, 265–271.
134. Wang, K.; Liu, Y.; Ding, Z.B.; Li, Y.Q.; Lu, T.; Pan, L.K. Metal-organic-frameworks-derived $NaTi_2(PO_4)_3$/carbon composites for efficient hybrid capacitive deionization. *J. Mater. Chem. A* **2019**, *7*, 12126–12133. [CrossRef]
135. Srimuk, P.; Lee, J.; Tolosa, A.; Kim, C.; Aslan, M.; Presser, V. Titanium disulfide: A promising low-dimensional electrode material for sodium ion intercalation for seawater desalination. *Chem. Mater.* **2017**, *29*, 9964–9973. [CrossRef]
136. Naguib, M.; Kurtoglu, M.; Presser, V.; Lu, J.; Niu, J.J.; Heon, M.; Hultman, L.; Gogotsi, Y.; Barsoum, M.W. Two-dimensional nanocrystals produced by exfoliation of Ti3AlC2. *Adv. Mater.* **2011**, *23*, 4248–4253.

137. Guo, L.; Wang, X.; Leong, Z.Y.; Mo, R.; Sun, L.; Yang, H.Y. Ar plasma modification of 2D MXene $Ti_3C_2T_x$ nanosheets for efficient capacitive desalination. *FlatChem* **2018**, *8*, 17–24. [CrossRef]
138. Ding, Z.; Xu, X.; Li, J.; Li, Y.; Wang, K.; Lu, T.; Hossain, M.S.A.; Amin, M.A.; Zhang, S.; Pan, L. Nanoarchitectonics from 2D to 3D: MXenes-derived nitrogen-doped 3D nanofibrous architecture for extraordinarily-fast capacitive deionization. *Chem. Eng. J.* **2022**, *430*, 133161. [CrossRef]
139. Giorgetti, M.; Scavetta, E.; Berrettoni, M.; Tonelli, D. Nickel hexacyanoferrate membrane as a coated wire cation-selective electrode. *Analyst* **2001**, *126*, 2168–2171.
140. Gao, X.; Omosebi, A.; Landon, J.; Liu, K.L. Surface charge enhanced carbon electrodes for stable and efficient capacitive deionization using inverted adsorption-desorption behavior. *Energy Environ. Sci.* **2015**, *8*, 897–909.
141. Karyakin, A.A. Prussian blue and its analogues: Electrochemistry and analytical applications. *Electroanalysis* **2001**, *13*, 813–819. [CrossRef]
142. Shi, W.; Liu, X.; Deng, T.; Huang, S.; Ding, M.; Miao, X.; Zhu, C.; Zhu, Y.; Liu, W.; Wu, F.; et al. Enabling superior sodium capture for efficient water desalination by a tubular polyaniline decorated with prussian blue nanocrystals. *Adv. Mater.* **2020**, *32*, 1907404. [CrossRef] [PubMed]
143. Neff, V.D. Electrochemical oxidation and reduction of thin films of prussian blue. *J. Electrochem. Soc.* **1978**, *125*, 886–887. [CrossRef]
144. Kim, S.; Lee, J.; Kang, J.S.; Jo, K.; Kim, S.; Sung, Y.-E.; Yoon, J. Lithium recovery from brine using a λ-MnO_2/activated carbon hybrid supercapacitor system. *Chemosphere* **2015**, *125*, 50–56. [CrossRef]
145. Zhang, H.; Zhao, Q.; Zhou, S.; Liu, N.; Wang, X.; Li, J.; Wang, F. Aqueous dispersed conducting polyaniline nanofibers: Promising high specific capacity electrode materials for supercapacitor. *J. Power Sources* **2011**, *196*, 10484–10489. [CrossRef]
146. Sultana, I.; Rahman, M.M.; Li, S.; Wang, J.; Wang, C.; Wallace, G.G.; Liu, H.-K. Electrodeposited polypyrrole (PPy)/para (toluene sulfonic acid) (pTS) free-standing film for lithium secondary battery application. *Electrochim. Acta* **2012**, *60*, 201–205. [CrossRef]
147. Zhang, J.; Shan, D.; Mu, S. A rechargeable Zn- poly(aniline-co-m-aminophenol) battery. *J. Power Sources* **2006**, *161*, 685–691. [CrossRef]
148. Hsu, H.-C.; Wang, C.-H.; Nataraj, S.K.; Huang, H.-C.; Du, H.-Y.; Chang, S.-T.; Chen, L.-C.; Chen, K.-H. Stand-up structure of graphene-like carbon nanowalls on CNT directly grown on polyacrylonitrile-based carbon fiber paper as supercapacitor. *Diam. Relat. Mater.* **2012**, *25*, 176–179. [CrossRef]
149. Shown, I.; Ganguly, A.; Chen, L.-C.; Chen, K.-H. Conducting polymer-based flexible supercapacitor. *Energy Sci. Eng.* **2015**, *3*, 2–26. [CrossRef]
150. Snook, G.A.; Kao, P.; Best, A.S. Conducting-polymer-based supercapacitor devices and electrodes. *J. Power Sources* **2011**, *196*, 1–12. [CrossRef]
151. Bandaru, P.R.; Yamada, H.; Narayanan, R.; Hoefer, M. Charge transfer and storage in nanostructures. *Mater. Sci. Eng. R Rep.* **2015**, *96*, 1–69. [CrossRef]
152. Amarnath, C.A.; Chang, J.H.; Kim, D.; Mane, R.S.; Han, S.-H.; Sohn, D. Electrochemical supercapacitor application of electroless surface polymerization of polyaniline nanostructures. *Mater. Chem. Phys.* **2009**, *113*, 14–17. [CrossRef]
153. Wang, H.; Hao, Q.; Yang, X.; Lu, L.; Wang, X. Graphene oxide doped polyaniline for supercapacitors. *Electrochem. Commun.* **2009**, *11*, 1158–1161. [CrossRef]
154. Zhang, X.; Goux, W.J.; Manohar, S.K. Synthesis of polyaniline nanofibers by "nanofiber seeding". *J. Am. Chem. Soc.* **2004**, *126*, 4502–4503. [CrossRef]
155. Liu, H.; Zhang, J.; Xu, X.; Wang, Q. A polyoxometalate-based binder-free capacitive deionization electrode for highly efficient sea water desalination. *Chem. Eur. J.* **2020**, *26*, 4403–4409. [CrossRef]
156. Lai, L.; Yang, H.; Wang, L.; Teh, B.K.; Zhong, J.; Chou, H.; Chen, L.; Chen, W.; Shen, Z.; Ruoff, R.S.; et al. Preparation of supercapacitor electrodes through selection of graphene surface functionalities. *ACS Nano* **2012**, *6*, 5941–5951. [CrossRef]
157. Yan, C.J.; Zou, L.; Short, R. Single-walled carbon nanotubes and polyaniline composites for capacitive deionization. *Desalination* **2012**, *290*, 125–129. [CrossRef]
158. Zhou, Y.; Qin, Z.-Y.; Li, L.; Zhang, Y.; Wei, Y.-L.; Wang, L.-F.; Zhu, M.-F. Polyaniline/multi-walled carbon nanotube composites with core–shell structures as supercapacitor electrode materials. *Electrochim. Acta* **2010**, *55*, 3904–3908. [CrossRef]
159. Fonner, J.M.; Schmidt, C.E.; Ren, P. A combined molecular dynamics and experimental study of doped polypyrrole. *Polymer* **2010**, *51*, 4985–4993. [CrossRef]
160. Killian, J.G.; Coffey, B.M.; Gao, F.; Poehler, T.O.; Searson, P.C. Polypyrrole composite electrodes in an all-polymer battery system. *J. Electrochem. Soc.* **1996**, *143*, 936–942. [CrossRef]
161. Wang, J.; Chen, J.; Wang, C.Y.; Zhou, D.; Too, C.O.; Wallace, G.G. Electrochemical synthesis of polypyrrole films using stainless steel mesh as substrate for battery application. *Synth. Met.* **2005**, *153*, 117–120. [CrossRef]
162. Ren, Y.Y.; Mao, X.W.; Hatton, T.A. An Asymmetric Electrochemical system with complementary tunability in hydrophobicity for selective separations of organics. *ACS Cent. Sci.* **2019**, *5*, 1396–1406. [CrossRef] [PubMed]
163. Ji, F.; Wang, L.; Yang, J.; Wu, X.; Li, M.; Jiang, S.; Lin, S.; Chen, Z. Highly compact, free-standing porous electrodes from polymer-derived nanoporous carbons for efficient electrochemical capacitive deionization. *J. Mater. Chem. A* **2019**, *7*, 1768–1778.
164. Ezika, A.C.; Sadiku, E.R.; Ray, S.S.; Hamam, Y.; Folorunso, O.; Adekoya, G.J. Emerging advancements in polypyrrole MXene hybrid nanoarchitectonics for capacitive energy storage applications. *J. Inorg. Organomet. Polym. Mater.* **2022**, *32*, 1521–1540. [CrossRef]

165. Su, X.; Kulik, H.J.; Jamison, T.F.; Hatton, T.A. Anion-selective redox electrodes: Electrochemically mediated separation with heterogeneous organometallic interfaces. *Adv. Funct. Mater.* **2016**, *26*, 3394–3404. [CrossRef]
166. Su, X.; Tan, K.J.; Elbert, J.; Ruttiger, C.; Gallei, M.; Jamison, T.F.; Hatton, T.A. Asymmetric Faradaic systems for selective electrochemical separations. *Energy Environ. Sci.* **2017**, *10*, 1272–1283. [CrossRef]
167. Su, X.; Kushima, A.; Halliday, C.; Zhou, J.; Li, J.; Hatton, T.A. Electrochemically-mediated selective capture of heavy metal chromium and arsenic oxyanions from water. *Nat. Commun.* **2018**, *9*, 4701. [CrossRef]
168. Ding, M.; Bannuru, K.K.R.; Wang, Y.; Guo, L.; Baji, A.; Yang, H.Y. Free-standing electrodes derived from metal–organic frameworks/nanofibers hybrids for membrane capacitive deionization. *Adv. Mater. Technol.* **2018**, *3*, 1800135.
169. Liu, Y.; Ma, J.Q.; Lu, T.; Pan, L.K. Electrospun carbon nanofibers reinforced 3D porous carbon polyhedra network derived from metal-organic frameworks for capacitive deionization. *Sci. Rep.* **2016**, *6*, 32784. [CrossRef]
170. Hussain, T.; Wang, Y.; Xiong, Z.; Yang, J.; Xie, Z.; Liu, J. Fabrication of electrospun trace NiO-doped hierarchical porous carbon nanofiber electrode for capacitive deionization. *J. Colloid Interface Sci.* **2018**, *532*, 343–351. [CrossRef]
171. Wang, G.; Dong, Q.; Wu, T.; Zhan, F.; Zhou, M.; Qiu, J. Ultrasound-assisted preparation of electrospun carbon fiber/graphene electrodes for capacitive deionization: Importance and unique role of electrical conductivity. *Carbon* **2016**, *103*, 311–317. [CrossRef]
172. Kim, T.; Dykstra, J.E.; Porada, S.; van der Wal, A.; Yoon, J.; Biesheuvel, P.M. Enhanced charge efficiency and reduced energy use in capacitive deionization by increasing the discharge voltage. *J. Colloid Interface Sci.* **2015**, *446*, 317–326. [CrossRef] [PubMed]
173. Kim, C.; Ko, C.J.; Leffell, D.J. Cutaneous squamous cell carcinomas of the lower extremity: A distinct subset of squamous cell carcinomas. *J. Am. Acad. Dermatol.* **2014**, *70*, 70–74. [CrossRef] [PubMed]
174. Zhao, R.; Porada, S.; Biesheuvel, P.M.; Van der Wal, A. Energy consumption in membrane capacitive deionization for different water recoveries and flow rates, and comparison with reverse osmosis. *Desalination* **2013**, *330*, 35–41. [CrossRef]
175. Kim, T.; Yoon, J. CDI ragone plot as a functional tool to evaluate desalination performance in capacitive deionization. *RSC Adv.* **2015**, *5*, 1456–1461. [CrossRef]
176. Jande, Y.A.C.; Kim, W.S. Desalination using capacitive deionization at constant current. *Desalination* **2013**, *329*, 29–34. [CrossRef]
177. Srinivasan, R.; Sorial, G.A. Treatment of perchlorate in drinking water: A critical review. *Sep. Purif. Technol.* **2009**, *69*, 7–21. [CrossRef]
178. Qu, Y.T.; Campbell, P.G.; Gu, L.; Knipe, J.M.; Dzenitis, E.; Santiago, J.G.; Stadermann, M. Energy consumption analysis of constant voltage and constant current operations in capacitive deionization. *Desalination* **2016**, *400*, 18–24. [CrossRef]
179. Chen, L.; Yin, X.; Zhu, L.; Qiu, Y. Energy recovery and electrode regeneration under different charge/discharge conditions in membrane capacitive deionization. *Desalination* **2018**, *439*, 93–101. [CrossRef]
180. Guo, H.; You, F.; Yu, S.; Li, L.; Zhao, D. Mechanisms of chemical cleaning of ion exchange membranes: A case study of plant-scale electrodialysis for oily wastewater treatment. *J. Membr. Sci.* **2015**, *496*, 310–317. [CrossRef]
181. Saleem, M.W.; Jande, Y.A.C.; Asif, M.; Kim, W.-S. Hybrid CV-CC operation of capacitive deionization in comparison with constant current and constant voltage. *Sep. Sci. Technol.* **2016**, *51*, 1063–1069. [CrossRef]
182. Cai, Y.; Wang, Y.; Han, X.; Zhang, L.; Xu, S.; Wang, J. Optimization on electrode assemblies based on ion-doped polypyrrole/carbon nanotube composite in capacitive deionization process. *J. Electroanal. Chem.* **2016**, *768*, 72–80. [CrossRef]
183. Steven, H.; Jeremy, G.; Roland, D. Technoeconomic analysis of brackish water capacitive deionization: Navigating tradeoffs between performance, lifetime, and material costs. *Environ. Sci. Technol.* **2019**, *53*, 13353–13363.
184. Lin, S. Energy Efficiency of desalination: Fundamental insights from intuitive interpretation. *Environ. Sci. Technol.* **2020**, *54*, 76–84. [CrossRef]
185. Park, J.S.; Song, J.H.; Yeon, K.H.; Moon, S.H. Removal of hardness ions from tap water using electromembrane processes. *Desalination* **2007**, *202*, 1–8. [CrossRef]
186. Gabrielli, C.; Maurin, G.; Francy-Chausson, H.; Thery, P.; Tran, T.T.M.; Tlili, M. Electrochemical water softening: Principle and application. *Desalination* **2006**, *201*, 150–163. [CrossRef]
187. Dean, J.G.; Bosqui, F.L.; Lanouette, K.H. Removing heavy metals from waste water. *Environ. Sci. Technol.* **1972**, *6*, 518–522. [CrossRef]
188. Nagarajan, M.K.; Paine, H.L. Water hardness control by detergent builders. *J. Am. Soc. Brew. Chem.* **1984**, *61*, 1475–1478.
189. Wiers, B.H.; Grosse, R.J.; Cilley, W.A. Divalent and trivalent ion exchange with zeolite A. *Environ. Sci. Technol.* **1982**, *16*, 617–624.
190. Ghizellaoui, S.; Chibani, A.; Ghizellaoui, S. Use of nanofiltration for partial softening of very hard water. *Desalination* **2005**, *179*, 315–322. [CrossRef]
191. Hauck, A.R.; Sourirajan, S. Performance of porous cellulose acetate membranes for the reverse osmosis treatment of hard and waste waters. *Environ. Sci. Technol.* **1969**, *3*, 1269–1275. [CrossRef]
192. Seo, S.-J.; Jeon, H.; Lee, J.K.; Kim, G.-Y.; Park, D.; Nojima, H.; Lee, J.; Moon, S.-H. Investigation on removal of hardness ions by capacitive deionization (CDI) for water softening applications. *Water Res.* **2010**, *44*, 2267–2275. [CrossRef] [PubMed]
193. Hou, C.-H.; Huang, C.-Y. A comparative study of electrosorption selectivity of ions by activated carbon electrodes in capacitive deionization. *Desalination* **2013**, *314*, 124–129. [CrossRef]
194. Aslani, P.; Kennedy, R.A. Studies on diffusion in alginate gels. I. Effect of cross-linking with calcium or zinc ions on diffusion of acetaminophen. *J. Control. Release* **1996**, *42*, 75–82. [CrossRef]
195. Chen, J.P.; Wang, L. Characterization of a Ca-alginate based ion-exchange resin and its applications in lead, copper, and zinc removal. *Sep. Sci. Technol.* **2001**, *36*, 3617–3637. [CrossRef]

196. Doornbusch, G.J.; Dykstra, J.E.; Biesheuvel, P.M.; Suss, M.E. Fluidized bed electrodes with high carbon loading for water desalination by capacitive deionization. *J. Mater. Chem. A* **2016**, *4*, 3642–3647. [CrossRef]
197. Fu, F.; Wang, Q. Removal of heavy metal ions from wastewaters: A review. *J. Environ. Manag.* **2011**, *92*, 407–418. [CrossRef]
198. Zhang, W.; Mossad, M.; Yazdi, J.S.; Zou, L. A statistical experimental investigation on arsenic removal using capacitive deionization. *Desalin. Water Treat.* **2016**, *57*, 3254–3260. [CrossRef]
199. Fan, C.-S.; Tseng, S.-C.; Li, K.-C.; Hou, C.-H. Electro-removal of arsenic (III) and arsenic (V) from aqueous solutions by capacitive deionization. *J. Hazard. Mater.* **2016**, *312*, 208–215. [CrossRef]
200. Lado, J.J.; Pérez-Roa, R.E.; Wouters, J.J.; Tejedor-Tejedor, M.I.; Anderson, M.A. Evaluation of operational parameters for a capacitive deionization reactor employing asymmetric electrodes. *Sep. Purif. Technol.* **2014**, *133*, 236–245. [CrossRef]
201. Zhang, X.; Yang, F.; Ma, J.; Liang, P. Effective removal and selective capture of copper from salty solution in flow electrode capacitive deionization. *Environ. Sci. Water Res. Technol.* **2020**, *6*, 341–350. [CrossRef]
202. Ma, J.; Zhang, Y.; Collins, R.N.; Tsarev, S.; Aoyagi, N.; Kinsela, A.S.; Jones, A.M.; Waite, T.D. Flow-electrode CDI removes the uncharged Ca–UO_2–CO_3 ternary complex from brackish potable groundwater: Complex dissociation, transport, and sorption. *Environ. Sci. Technol.* **2019**, *53*, 2739–2747. [CrossRef] [PubMed]
203. Zhao, Y.; Wu, M.; Shen, P.; Uytterhoeven, C.; Mamrol, N.; Shen, J.; Gao, C.; Van der Bruggen, B. Composite anti-scaling membrane made of interpenetrating networks of nanofibers for selective separation of lithium. *J. Membr. Sci.* **2021**, *618*, 118668. [CrossRef]
204. Liu, L.; Qiu, G.; Suib, S.L.; Liu, F.; Zheng, L.; Tan, W.; Qin, L. Enhancement of Zn^{2+} and Ni^{2+} removal performance using a deionization pseudocapacitor with nanostructured birnessite and its carbon nanotube composite electrodes. *Chem. Eng. J.* **2017**, *328*, 464–473. [CrossRef]
205. Liu, L.H.; Peng, Q.C.; Qiu, G.H.; Zhu, J.; Tan, W.F.; Liu, C.S.; Zheng, L.R.; Dang, Z. Cd^{2+} adsorption performance of tunnel-structured manganese oxides driven by electrochemically controlled redox. *Environ. Pollut.* **2019**, *244*, 783–791. [CrossRef] [PubMed]
206. Wang, R.Y.; Shyam, B.; Stone, K.H.; Weker, J.N.; Pasta, M.; Lee, H.-W.; Toney, M.F.; Cui, Y. Reversible multivalent (monovalent, divalent, trivalent) ion insertion in open framework materials. *Adv. Energy Mater.* **2015**, *5*, 1401869. [CrossRef]
207. Zhang, Y.; Xue, Q.; Li, F.; Dai, J. Removal of heavy metal ions from wastewater by capacitive deionization using polypyrrole/chitosan composite electrode. *Adsorpt. Sci. Technol.* **2019**, *37*, 205–216. [CrossRef]
208. Zhang, Y.J.; Xue, J.Q.; Li, F.; Dai, J.Z.; Zhang, X.Z.Y. Preparation of polypyrrole/chitosan/carbon nanotube composite nano-electrode and application to capacitive deionization process for removing Cu^{2+}. *Chem. Eng. Process.* **2019**, *139*, 121–129. [CrossRef]
209. Dugas, R.; Rochelle, G. Absorption and desorption rates of carbon dioxide with monoethanolamine and piperazine. *Energy Procedia* **2009**, *1*, 1163–1169. [CrossRef]
210. Conway, W.; Wang, X.; Fernandes, D.; Burns, R.; Lawrance, G.; Puxty, G.; Maeder, M. Comprehensive Kinetic and Thermodynamic Study of the Reactions of CO_2(aq) and HCO_3^- with Monoethanolamine (MEA) in Aqueous Solution. *J. Phys. Chem. A* **2011**, *115*, 14340–14349. [CrossRef]
211. Pera-Titus, M. Porous inorganic membranes for CO_2 capture: Present and prospects. *Chem. Rev.* **2014**, *114*, 1413–1492. [CrossRef] [PubMed]
212. Ramasubramanian, K.; Verweij, H.; Winston Ho, W.S. Membrane processes for carbon capture from coal-fired power plant flue gas: A modeling and cost study. *J. Membr. Sci.* **2012**, *421–422*, 299–310. [CrossRef]
213. Datta, S.; Henry, M.P.; Lin, Y.J.; Fracaro, A.T.; Millard, C.S.; Snyder, S.W.; Stiles, R.L.; Shah, J.; Yuan, J.; Wesoloski, L.; et al. Electrochemical CO_2 capture using resin-wafer electrodeionization. *Ind. Eng. Chem. Res.* **2013**, *52*, 15177–15186. [CrossRef]
214. Eisaman, M.D.; Alvarado, L.; Larner, D.; Wang, P.; Garg, B.; Littau, K.A. CO_2 separation using bipolar membrane electrodialysis. *Energy Environ. Sci.* **2011**, *4*, 1319–1328. [CrossRef]
215. Kokoszka, B.; Jarrah, N.K.; Liu, C.; Moore, D.T.; Landskron, K. Supercapacitive swing adsorption of carbon dioxide. *Angew. Chem. Int. Ed.* **2014**, *53*, 3698–3701. [CrossRef]
216. Ozdemir, E. Biomimetic CO_2 Sequestration: 1. Immobilization of carbonic anhydrase within polyurethane foam. *Energy Fuels* **2009**, *23*, 5725–5730. [CrossRef]
217. Yadav, R.; Wanjari, S.; Prabhu, C.; Kumar, V.; Labhsetwar, N.; Satyanarayanan, T.; Kotwal, S.; Rayalu, S. Immobilized carbonic anhydrase for the biomimetic carbonation reaction. *Energy Fuels* **2010**, *24*, 6198–6207. [CrossRef]
218. Dai, N.; Shah, A.D.; Hu, L.; Plewa, M.J.; McKague, B.; Mitch, W.A. Measurement of nitrosamine and nitramine formation from NO_x reactions with amines during amine-based carbon dioxide capture for postcombustion carbon sequestration. *Environ. Sci. Technol.* **2012**, *46*, 9793–9801. [CrossRef]
219. Lepaumier, H.; da Silva, E.F.; Einbu, A.; Grimstvedt, A.; Knudsen, J.N.; Zahlsen, K.; Svendsen, H.F. Comparison of MEA degradation in pilot-scale with lab-scale experiments. *Energy Procedia* **2011**, *4*, 1652–1659. [CrossRef]
220. da Silva, E.F.; Lepaumier, H.; Grimstvedt, A.; Vevelstad, S.J.; Einbu, A.; Vernstad, K.; Svendsen, H.F.; Zahlsen, K. Understanding 2-ethanolamine degradation in postcombustion CO_2 capture. *Ind. Eng. Chem. Res.* **2012**, *51*, 13329–13338. [CrossRef]
221. Wagner, E.D.; Hsu, K.-M.; Lagunas, A.; Mitch, W.A.; Plewa, M.J. Comparative genotoxicity of nitrosamine drinking water disinfection byproducts in Salmonella and mammalian cells. *Mutat. Res.* **2012**, *741*, 109–115. [CrossRef] [PubMed]
222. Martin, S.; Lepaumier, H.; Picq, D.; Kittel, J.; de Bruin, T.; Faraj, A.; Carrette, P.-L. New amines for CO_2 capture. IV. degradation, corrosion, and quantitative structure property relationship model. *Ind. Eng. Chem. Res.* **2012**, *51*, 6283–6289. [CrossRef]

223. Sun, Y.; Wang, Q.; Wang, Y.; Yun, R.; Xiang, X. Recent advances in magnesium/lithium separation and lithium extraction technologies from salt lake brine. *Sep. Purif. Technol.* **2021**, *256*, 117807. [CrossRef]
224. Xu, W.; He, L.; Zhao, Z. Lithium extraction from high Mg/Li brine via electrochemical intercalation/de-intercalation system using $LiMn_2O_4$ materials. *Desalination* **2021**, *503*, 114935. [CrossRef]
225. Meng, F.; McNeice, J.; Zadeh, S.S.; Ghahreman, A. Review of lithium production and recovery from minerals, brines, and lithium-ion batteries. *Miner. Process. Extr. Metall. Rev.* **2021**, *42*, 123–141. [CrossRef]
226. Hoshino, T. Development of technology for recovering lithium from seawater by electrodialysis using ionic liquid membrane. *Fusion Eng. Des.* **2013**, *88*, 2956–2959. [CrossRef]
227. Mohr, S.H.; Mudd, G.M.; Giurco, D. Lithium resources and production: Critical assessment and global projections. *Minerals* **2012**, *2*, 65–84. [CrossRef]
228. Flexer, V.; Fernando Baspineiro, C.; Ines Galli, C. Lithium recovery from brines: A vital raw material for green energies with a potential environmental impact in its mining and processing. *Sci. Total Environ.* **2018**, *639*, 1188–1204. [CrossRef]
229. Battistel, A.; Palagonia, M.S.; Brogioli, D.; La Mantia, F.; Trocoli, R. Electrochemical methods for lithium recovery: A comprehensive and critical review. *Adv. Mater.* **2020**, *32*, 1905440. [CrossRef]
230. Swain, B.J.S. Recovery and recycling of lithium: A review. *Sep. Purif. Technol.* **2017**, *172*, 388–403. [CrossRef]
231. Kumar, A.; Fukuda, H.; Hatton, T.A.; Lienhard, J.H.V. Lithium recovery from oil and gas produced water: A need for a growing energy industry. *ACS Energy Lett.* **2019**, *4*, 1471–1474. [CrossRef]
232. Bajestani, M.B.; Moheb, A.; Dinari, M. Preparation of lithium ion-selective cation exchange membrane for lithium recovery from sodium contaminated lithium bromide solution by electrodialysis process. *Desalination* **2020**, *486*, 114476. [CrossRef]
233. Gamaethiralalage, J.G.; Singh, K.; Sahin, S.; Yoon, J.; Elimelech, M.; Suss, M.E.; Liang, P.; Biesheuvel, P.M.; Zornitta, R.L.; de Smet, L.C.P.M. Recent advances in ion selectivity with capacitive deionization. *Energy Environ. Sci.* **2021**, *14*, 1095–1120. [CrossRef]
234. Siekierka, A.; Kujawa, J.; Kujawski, W.; Bryjak, M. Lithium dedicated adsorbent for the preparation of electrodes useful in the ion pumping method. *Sep. Purif. Technol.* **2018**, *194*, 231–238. [CrossRef]
235. Missoni, L.L.; Marchini, F.; del Pozo, M.; Calvo, E.J. A $LiMn_2O_4$-polypyrrole system for the extraction of LiCl from natural brine. *J. Electrochem. Soc.* **2016**, *163*, A1898–A1902. [CrossRef]
236. Marchini, F.; Rubi, D.; del Pozo, M.; Williams, F.J.; Calvo, E.J. Surface chemistry and lithium-ion exchange in $LiMn_2O_4$ for the electrochemical selective extraction of LiCl from natural salt lake brines. *J. Phys. Chem. C* **2016**, *120*, 15875–15883. [CrossRef]
237. Zhao, Z.; Si, X.; Liu, X.; He, L.; Liang, X. Li extraction from high Mg/Li ratio brine with $LiFePO_4/FePO_4$ as electrode materials. *Hydrometallurgy* **2013**, *133*, 75–83. [CrossRef]
238. Liu, X.; Chen, X.; Zhao, Z.; Liang, X. Effect of Na^+ on Li extraction from brine using $LiFePO_4/FePO_4$ electrodes. *Hydrometallurgy* **2014**, *146*, 24–28. [CrossRef]
239. Meshram, P.; Pandey, B.D.; Mankhand, T.R. Recovery of valuable metals from cathodic active material of spent lithium ion batteries: Leaching and kinetic aspects. *Waste Manag.* **2015**, *45*, 306–313. [CrossRef]
240. Moazeni, M.; Hajipour, H.; Askari, M.; Nusheh, M. Hydrothermal synthesis and characterization of titanium dioxide nanotubes as novel lithium adsorbents. *Mater. Res. Bull.* **2015**, *61*, 70–75. [CrossRef]
241. Zhang, L.; Zhou, D.; He, G.; Yao, Q.; Wang, F.; Zhou, J. Synthesis of $H_2TiO_3^-$ lithium adsorbent loaded on ceramic foams. *Mater. Lett.* **2015**, *145*, 351–354. [CrossRef]
242. Siekierka, A. Lithium and magnesium separation from brines by hybrid capacitive deionization. *Desalination* **2022**, *527*, 115569. [CrossRef]
243. Siekierka, A. Lithium iron manganese oxide as an adsorbent for capturing lithium ions in hybrid capacitive deionization with different electrical modes. *Sep. Purif. Technol.* **2020**, *236*, 116234. [CrossRef]
244. Jin, W.; Hu, M.; Sun, Z.; Huang, C.-H.; Zhao, H. Simultaneous and precise recovery of lithium and boron from salt lake brine by capacitive deionization with oxygen vacancy-rich $CoP/Co_3O_4^-$ graphene aerogel. *Chem. Eng. J.* **2021**, *420*, 127661. [CrossRef]
245. Chen, L.; Gu, Q.; Zhou, X.; Lee, S.; Xia, Y.; Liu, Z. New-concept batteries based on aqueous Li^+/Na^+ mixed-ion electrolytes. *Sci. Rep.* **2013**, *3*, 1946. [CrossRef]
246. Zhao, M.-Y.; Ji, Z.-Y.; Zhang, Y.-G.; Guo, Z.-Y.; Zhao, Y.-Y.; Liu, J.; Yuan, J.-S. Study on lithium extraction from brines based on $LiMn_2O_4/Li_{1-x}Mn_2O_4$ by electrochemical method. *Electrochim. Acta* **2017**, *252*, 350–361. [CrossRef]
247. Kim, J.-S.; Lee, Y.-H.; Choi, S.; Shin, J.; Dinh, H.-C.; Choi, J.W. An electrochemical cell for selective lithium capture from seawater. *Environ. Sci. Technol.* **2015**, *49*, 9415–9422. [CrossRef]
248. Neufeld, R.D.; Thodos, G. Removal of orthophosphates from aqueous solutions with activated alumina. *Environ. Sci. Technol.* **1969**, *3*, 661–667. [CrossRef]
249. Cordell, D.; Rosemarin, A.; Schröder, J.J.; Smit, A.L. Towards global phosphorus security: A systems framework for phosphorus recovery and reuse options. *Chemosphere* **2011**, *84*, 747–758. [CrossRef]
250. Zuthi, M.F.R.; Guo, W.S.; Ngo, H.H.; Nghiem, L.D.; Hai, F.I. Enhanced biological phosphorus removal and its modeling for the activated sludge and membrane bioreactor processes. *Bioresour. Technol.* **2013**, *139*, 363–374. [CrossRef]
251. Bian, Y.; Chen, X.; Lu, L.; Liang, P.; Ren, Z.J. Concurrent nitrogen and phosphorus recovery using flow-electrode capacitive deionization. *ACS Sustain. Chem. Eng.* **2019**, *7*, 7844–7850. [CrossRef]
252. Zhang, C.; Ma, J.; Waite, T.D. Ammonia-rich solution production from wastewaters using chemical-free flow-electrode capacitive deionization. *ACS Sustain. Chem. Eng.* **2019**, *7*, 6480–6485. [CrossRef]

253. Zhang, C.; Ma, J.; Song, J.; He, C.; Waite, T.D. Continuous ammonia recovery from wastewaters using an integrated capacitive flow electrode membrane stripping system. *Environ. Sci. Technol.* **2018**, *52*, 14275–14285. [CrossRef] [PubMed]
254. Kf, A.; Whb, A.; Fei, P.; Kw, A. Ammonia recovery from concentrated solution by designing novel stacked FCDI cell. *Sep. Purif. Technol.* **2020**, *250*, 117066.
255. Kim, T.; Gorski, C.A.; Logan, B.E. Ammonium removal from domestic wastewater using selective battery electrodes. *Environ. Sci. Technol. Lett.* **2018**, *5*, 578. [CrossRef]
256. Yoon, H.; Lee, J.; Kim, S.; Yoon, J. Review of concepts and applications of electrochemical ion separation (EIONS) process. *Sep. Purif. Technol.* **2019**, *215*, 190–207. [CrossRef]
257. Yeo, J.-H.; Choi, J.-H. Enhancement of nitrate removal from a solution of mixed nitrate, chloride and sulfate ions using a nitrate-selective carbon electrode. *Desalination* **2013**, *320*, 10–16. [CrossRef]
258. Zhang, C.; Ma, J.; He, D.; Waite, T.D. Capacitive membrane stripping for ammonia recovery (CapAmm) from dilute wastewaters. *Environ. Sci. Technol. Lett.* **2018**, *5*, 43–49. [CrossRef]
259. Li, Y.; Zhang, C.; Jiang, Y.; Wang, T.-J.; Wang, H. Effects of the hydration ratio on the electrosorption selectivity of ions during capacitive deionization. *Desalination* **2016**, *399*, 171–177. [CrossRef]
260. Chen, Z.; Zhang, H.; Wu, C.; Wang, Y.; Li, W. A study of electrosorption selectivity of anions by activated carbon electrodes in capacitive deionization. *Desalination* **2015**, *369*, 46–50. [CrossRef]
261. Dodds, W.K.; Bouska, W.W.; Eitzmann, J.L.; Pilger, T.J.; Pitts, K.L.; Riley, A.J.; Schloesser, J.T.; Thornbrugh, D.J. Eutrophication of U.S. freshwaters: Analysis of potential economic damages. *Environ. Sci. Technol.* **2009**, *43*, 12–19. [CrossRef] [PubMed]
262. Zhang, J.; Tang, L.; Tang, W.; Zhong, Y.; Luo, K.; Duan, M.; Xing, W.; Liang, J. Removal and recovery of phosphorus from low-strength wastewaters by flow-electrode capacitive deionization. *Sep. Purif. Technol.* **2020**, *237*, 116322. [CrossRef]
263. Zhang, C.; Wang, M.; Xiao, W.; Ma, J.; Sun, J.; Mo, H.; Waite, T.D. Phosphate selective recovery by magnetic iron oxide impregnated carbon flow-electrode capacitive deionization (FCDI). *Water Res.* **2021**, *189*, 116653. [CrossRef] [PubMed]
264. Zhang, C.; Cheng, X.; Wang, M.; Ma, J.; Collins, R.; Kinsela, A.; Zhang, Y.; Waite, T.D. Phosphate recovery as vivianite using a flow-electrode capacitive desalination (FCDI) and fluidized bed crystallization (FBC) coupled system. *Water Res.* **2021**, *194*, 116939. [CrossRef]
265. Xu, L.; Ding, R.; Mao, Y.; Peng, S.; Li, Z.; Zong, Y.; Wu, D. Selective recovery of phosphorus and urea from fresh human urine using a liquid membrane chamber integrated flow-electrode electrochemical system. *Water Res.* **2021**, *202*, 117423. [CrossRef]
266. Tao, G.; Viswanath, B.; Kekre, K.; Lee, L.Y.; Ng, H.Y.; Ong, S.L.; Seah, H. RO brine treatment and recovery by biological activated carbon and capacitive deionization process. *Water Sci. Technol.* **2011**, *64*, 77–82. [CrossRef]
267. Ye, G.; Yu, Z.; Li, Y.; Li, L.; Song, L.; Gu, L.; Cao, X. Efficient treatment of brine wastewater through a flow-through technology integrating desalination and photocatalysis. *Water Res.* **2019**, *157*, 134–144. [CrossRef]
268. Feng, C.; Hou, C.-H.; Chen, S.; Yu, C.-P. A microbial fuel cell driven capacitive deionization technology for removal of low level dissolved ions. *Chemosphere* **2013**, *91*, 623–628. [CrossRef]
269. Panagopoulos, A.; Haralambous, K.-J.; Loizidou, M. Desalination brine disposal methods and treatment technologies—A review. *Sci. Total Environ.* **2019**, *693*, 133545. [CrossRef]
270. Mavukkandy, M.O.; Chabib, C.M.; Mustafa, I.; Al Ghaferi, A.; AlMarzooqi, F. Brine management in desalination industry: From waste to resources generation. *Desalination* **2019**, *472*, 114187. [CrossRef]
271. Yu, J.; Qin, J.; Kekre, K.A.; Viswanath, B.; Tao, G.; Seah, H. Impact of operating conditions on performance of capacitive deionisation for reverse osmosis brine recovery. *J. Water Reuse Desalin.* **2013**, *4*, 59–64. [CrossRef]
272. Minhas, M.B.; Jande, Y.A.C.; Kim, W.S. Combined reverse osmosis and constant—current operated capacitive deionization system for seawater desalination. *Desalination* **2014**, *344*, 299–305. [CrossRef]
273. Chung, H.J.; Kim, J.; Kim, D.I.; Gwak, G.; Hong, S. Feasibility study of reverse osmosis-flow capacitive deionization (RO-FCDI) for energy-efficient desalination using seawater as the flow-electrode aqueous electrolyte. *Desalination* **2020**, *479*, 114326. [CrossRef]
274. Ma, R.; Zhang, S.; Wen, T.; Gu, P.; Li, L.; Zhao, G.; Niu, F.; Huang, Q.; Tang, Z.; Wang, X. A critical review on visible-light-response CeO_2-based photocatalysts with enhanced photooxidation of organic pollutants. *Catal. Today* **2019**, *335*, 20–30. [CrossRef]
275. Pi, Y.; Li, X.; Xia, Q.; Wu, J.; Li, Y.; Xiao, J.; Li, Z. Adsorptive and photocatalytic removal of persistent organic pollutants (POPs) in water by metal-organic frameworks (MOFs). *Chem. Eng. J.* **2018**, *337*, 351–371. [CrossRef]
276. Zhang, Y.; Liu, M.; Zhou, M.; Yang, H.; Liang, L.; Gu, T. Microbial fuel cell hybrid systems for wastewater treatment and bioenergy production: Synergistic effects, mechanisms and challenges. *Renew. Sust. Energ. Rev.* **2019**, *103*, 13–29. [CrossRef]
277. Yamashita, T.; Hayashi, T.; Iwasaki, H.; Awatsu, M.; Yokoyama, H. Ultra-low-power energy harvester for microbial fuel cells and its application to environmental sensing and long-range wireless data transmission. *J. Power Sources* **2019**, *430*, 1–11. [CrossRef]
278. Forrestal, C.; Xu, P.; Ren, Z. Sustainable desalination using a microbial capacitive desalination cell. *Energy Environ. Sci.* **2012**, *5*, 7161–7167. [CrossRef]
279. Forrestal, C.; Stoll, Z.; Xu, P.; Ren, Z.J. Microbial capacitive desalination for integrated organic matter and salt removal and energy production from unconventional natural gas produced water. *Environ. Sci. Water Res. Technol.* **2015**, *1*, 47–55. [CrossRef]